Available online at www.sciencedirect.com

ScienceDirect

Advances in Space Research 77 (2026) 4864–4884

ADVANCES IN SPACE RESEARCH (a COSPAR publication)

www.elsevier.com/locate/asr

Space debris index definition for multi-purpose active debris removal mission design

Giacomo Borelli *, Camilla Colombo

Politecnico di Milano, via La Masa 34, 20156 Milan, Italy

Received 12 February 2025; received in revised form 12 December 2025; accepted 16 December 2025
Available online 19 December 2025

Abstract

Recent advances in space debris mitigation methods have become a prominent area of research and interest within the space community. Active debris removal missions are widely recognized as essential for improving both current and future debris conditions and promoting the sustainable use of near-Earth space. This paper introduces a novel method for studying and characterizing debris objects as potential targets for multiple Active Debris Removal (ADR) missions. A detailed framework for evaluating the impact factor of debris, considering both mission feasibility and environmental impact, is provided. This approach is integrated into a flexible mission design tool that leverages a multi-objective optimization algorithm to generate potential missions, enabling the selection of optimal debris targets based on specific needs. Simulation results for three separate mission cases are presented in this paper that optimally select targets for a multiple ARD mission service in Low Earth Orbit (LEO).

Keywords: Space debris mitigation; Active debris removal; Mission design; Optimisation

1. Introduction

The growth of man-made objects in space around Earth is rising concerns among the space community. Sustainability and future use of outer space for scientific and commercial goals keeps being endangered by the growing problem of space debris. These uncontrolled objects and fragments pose a substantial threat to the current population of active satellite operated around Earth, which as of now they have to implement counteracting measures such as avoidance manoeuvres to avoid catastrophic events of collision. A snapshot of the current situation of the debris and space environment is outlined in the Space Environment Report (ESA Space Debris Office, 2024), issued by the European Space Agency (ESA), where these problematic are highlighted in a quantitative way. Furthermore, the effect of the current debris population is described both in terms of required collision avoidance measures and unwanted collisions. In summary, the growth of the number of debris is worrying the experts for the possible uncontrolled growth due to a cascade collision effect, and the operators for the increase number of collision avoidance manoeuvres from satellites in certain regions. To mitigate these effects, the number of uncontrolled debris objects must be reduced and controlled in the future. A possible mitigation strategy is identified by the space community in actively removing objects from space, which will avoid their further collisions/fragmentation and will reduce the risk of debris population growth in the future. In Liou and Johnson (2009, 2011) it was concluded, that with at least a rate of removal of five objects per year the growth of debris population in LEO can be largely mitigated and eventually stopped. Indeed, these removal rates were found to be effective under the environmental conditions of the past but may

* Corresponding author.
E-mail addresses: giacomo.borelli@polimi.it (G. Borelli), camilla.colombo@polimi.it (C. Colombo).

https://doi.org/10.1016/j.asr.2025.12.059
0273-1177/

become ineffective for the more recent debris population. The question of how many removals are needed to stabilize the long-term evolution of the environment remains an active area of research Giudici et al. (2024).

Solutions for the feasibility and applicability of Active Debris Removal (ADR) missions to manage the in-orbit debris population have been actively pursued by the space community over the past decades. Significant technological challenges exist in approaching and removing uncooperative, non-collaborative objects, and no mission has successfully performed a debris removal to date. Several methods in literature are proposed, from the use of robotic arms (Biesbroek et al., 2017; Jaekel et al., 2018) and tethered nets and harpoons (Forshaw et al., 2016), to contactless methods, such as laser ablation (Tsuno et al., 2022), ion beams (Bombardelli and Pelaez, 2011) and electrostatic forces (Schaub and Sternosvky, 2013). A notable example in literature is represented by the ESA funded e.Deorbit mission study (Biesbroek et al., 2017) which reached up to phase B and aimed to capture and remove with a robotic arm the large uncontrolled satellite ENVISAT. Currently, the ClearSpace-1 mission is venturing to design a satellite with multiple manipulators to capture and remove a debris object Biesbroek et al. (2021). Furthermore, Japan Aerospace and Exploration Agency (JAXA) is active in the development of ADR mission and technologies. It is currently implementing the Commercial Removal of Debris Demonstration (CDR-2) programme which aims to establish ADR as a new business thorough funding of missions in cooperation with private companies. The first mission of the programme, ADRAS-J, achieved rendezvous to a derelict rocket bodies, performing proximity operations and inspection at distances up to 50 meters (Atarashi et al., 2024).

A future direction of sustainable space activities and logistic will be to have ADR missions as a service, which can act to mitigate collision risks in required orbital regions, jointly with the plethora of other mitigation measure present. The future question to the community will be raised on the topic of selection of target objects to be removed that can mostly benefit the space envirnoment and future operations. The objective of this paper is twofold. Firstly, a comprehensive framework to rank the debris population is presented, specifically tailored to ADR targets and their peculiarities relevant for removal missions. Secondly, a flexible mission design tool is developed which optimally selects the targets to remove within an ADR service accounting for the overall benefit to the environment and the mission cost.

Several studies in literature have focused on the target selection and mission planning problem for removal missions. Of specific interest are the multiple ADR mission architectures, where multiple targets can be sequentially removed within the same mission, hence increasing the effectiveness per launch. Within this field, the literature focused on the optimisation of the sequence of debris to minimise a mission metric, typically identified with the propellant expenditure or mission time (or a combination of the two).

Bérend and Olive (2016) approached the problem of selecting 10 debris using a 15 tons servicer by performing a bi-objective optimisation considering the propellant consumption and the total time of flight. In the aforementioned work, the authors used a branch and bound algorithm to tackle the optimisation problem and considered two separate disposal strategies: (1) direct servicer + debris transfer to disposal orbit, (2) servicer attaches a deorbiting kit to the debris. A branch and bound algorithm was used also by the reference Cerf (2013), where impulsive transfers are considered and the simultaneous optimisation of the sequence selection and orbital manoeuvres is done. Also Madakat et al. (2013) solved the bi-objective optimisation problem minimising the propellant consumption and transfer time with a branch and bound algorithm. Casalino used an evolutionary to optimise the impulsive transfers to remove the Russian Kosmos 3 M rockets residing in the 82 degrees inclination slot in LEO. A simulated annealing is used to solve the problem of removal of 20 targets in Federici et al. (2019a). Machine learning methods are explored in Xu et al. (2023), where an estimation method for approximating the impulsive delta-v required for the transfers based on deep neural networks coupled with a reinforcement learning method for optimising the sequence of debris is used. Neural networks approximation of the transfer costs are studied also in Viavattene et al. (2022), which achieved a great reduction of computational time of the sequence optimisation problem. Genetic algorithms have been used to solve this problem in literature (Murakami and Hokamoto, 2010; Federici et al., 2019b; Liu and Yang). In Federici et al. (2021) an A* algorithm was applied to the debris sequence optimisation of a debris cluster in Sun synchronous orbit. The authors in reference Shen et al. (2018) exploited a evolutionary algorithm, namely an ant colony optimisation, to prove that the removal of around four to six objects at similar inclinations is feasible with current chemical and electric propulsion technology. Low thrust approaches for the transfers between debris are explored in the reference Zuiani and Vasile (2012), where a simplified and fast low thrust multi-revolution design algorithm is used within a multi-objective optimisation problem of sequence selection minimising the propellant and total mission time. In reference Carlo et al. (2017) the optimisation of debris sequence between 800 and 1400 km of altitude is done minimising the delta-v expenditure for low thrust transfers using a bio-inspired optimisation algorithm.

The target selection for an multiple ADR mission can be re-conducted to a travelling salesman problem (TSP), which has a combinatorial nature and is an NP-hard problem. Therefore, the dynamics and transfer models between targets, both considering impulsive and low-thrust approaches, relied on simplified approaches.

Remarking the relevance and complexity of the topic, the optimisation problem of debris sequence selection

under J_2 perturbed near-Earth orbital dynamics has been proposed in 2014 during the GTOC 9 competition and named "The Kessler Run" (Izzo and Maertens, 2018). Within this event, several teams around the world have proposed solutions to the impulsive transfers to an optimal sequence of debris in LEO by minimising a cost function related to the mission delta-v cost, total mission time, and, as common for these competition events, the solution's delivery time (Petropoulos et al., 2018; Izzo and Maertens, 2018; Hallmann et al., 2017).

The aforementioned works predominantly focus on identifying solutions aimed at minimizing propellant consumption for the servicer and reducing the total mission duration, as these factors typically drive the costs in space mission design. Nevertheless, when dealing with the peculiar problem of multiple ADR mission design, the minimisation/maximisation of different cost metrics of the sequence can be of great interest. For example the maximisation of the impact on the long term debris environment evolution through the removal of objects as mitigation strategy can align mission design to the broader objective of multiple ADR mission. In fact, within a sequence of debris which results optimal for the servicer propellant consumption, it might be that there are few targets whose removal is not as of interest as for other targets or their feasibility is not possible.

Authors in the field have started to address also these aspects. Liu and Yang Liu and Yang performed a bi-objective optimisation through an evolutionary algorithm obtaining pareto solutions with mission cost and collision risks as the key cost metrics. Yang et al. Yang et al. (2018) took a different approach by maximising the total reward of the removed objects and imposing delta-v and total mission time as constraints. The reward function used is based on the potential risk of the removed objects to operational spacecraft. A greedy heuristic is then applied to solve the optimal sequence among the Iridium 33 debris cloud data. In a similar way, the authors in Barea et al. (2020) also exploit the maximisation of the cumulative impact of the removal of a sequence of debris, modelled through the Criticality of Spacecraft Index (CSI) of reference Rossi et al. (2015a). Once again the delta-v and total mission time are imposed as constraints.

In this paper, the problem is considered first by an analysis and a identification of the impact factor of interest for a ADR mission, developing a multi-index ranking framework that quantify the advantages and complexities of removing each debris objects in orbit. Specifically, the aspects under study include: (1) the criticality of an object to the debris environment in terms of collision risk and fragments generated in case of a collision, (2) the complexities of performing removal operations with rigid capture to particular objects, and (3) the benefit from a commercial perspective of clearing a certain objects from a valuable orbital slot. These impact factors are then used to compute a cumulative metric, called the ADR index, which is optimized jointly with mission cost quantities (e.g., propellant) within a mission design tool to determine the optimal sequence of removals.

This paper is organised as follows: after this introduction, a study of the current debris population characteristics is presented, with focus in the orbital region and properties relevant for ADR missions. Subsequently, the definition of the ADR index is outlined in Section 3. Section 5 describe the multi-objective mission design tool developed to solve the multiple ADR design. The results of three different test cases are presented and discussed in Section 6, where ADR missions with different capabilities and objectives are considered. Finally, conclusion are drawn to highlight the achievement of the approach and future development plans and possibility of the methods are outlined.

2. Debris population analysis

According to the ESA Annual Space Environment Report of 2024 ESA Space Debris Office (2024), which provides statistics on the space environment up to the end of 2023, more than 35,000 objects are currently being tracked around Earth. Of these, approximately 9,100 are active payloads, while the remainder are debris larger than 10 cm. It is also estimated that debris larger than 1 cm exceeds one million in number.

The majority of the data used in this paper was retrieved from the ESA DISCOS database Floher et al. (2013, 2023), where debris objects are categorized into different types: payload, payload mission-related objects, payload fragmentation debris, payload debris, rocket body, rocket body mission-related objects, rocket fragmentation debris, and rocket debris. Additionally, the physical characteristics of the debris, such as fundamental dimensions, mass, shape, and cross-sectional area (average, minimum, and maximum), are reported. The orbital data for each classified debris object in the DISCOS database was obtained as Two-Line Elements (TLEs) from SpaceTrack SpaceTrack (2023).

Figs. 1a and 1b show the distribution of space debris objects in the LEO region, representing the cumulative mass and object count in terms of semi-major axis and inclination, respectively. Several high-density regions of debris are already identifiable. For example, the band around 90–100 degrees of inclination corresponds to the Sun-Synchronous Orbit (SSO) region, which has been of great interest for launches and missions across various applications, resulting in high traffic over recent years.

In addition to their orbital location and physical characteristics, other properties of debris objects significantly influence the planning and operations of an ADR mission. Specifically, the dynamic state of an object, i.e. its rotational motion, is often crucial in determining the feasibility of capture and removal. In missions involving rigid or contact-based capture methods, rapid rotational motion can impose severe constraints and complications in safely capturing and stabilizing the debris. Unfortunately, accu-

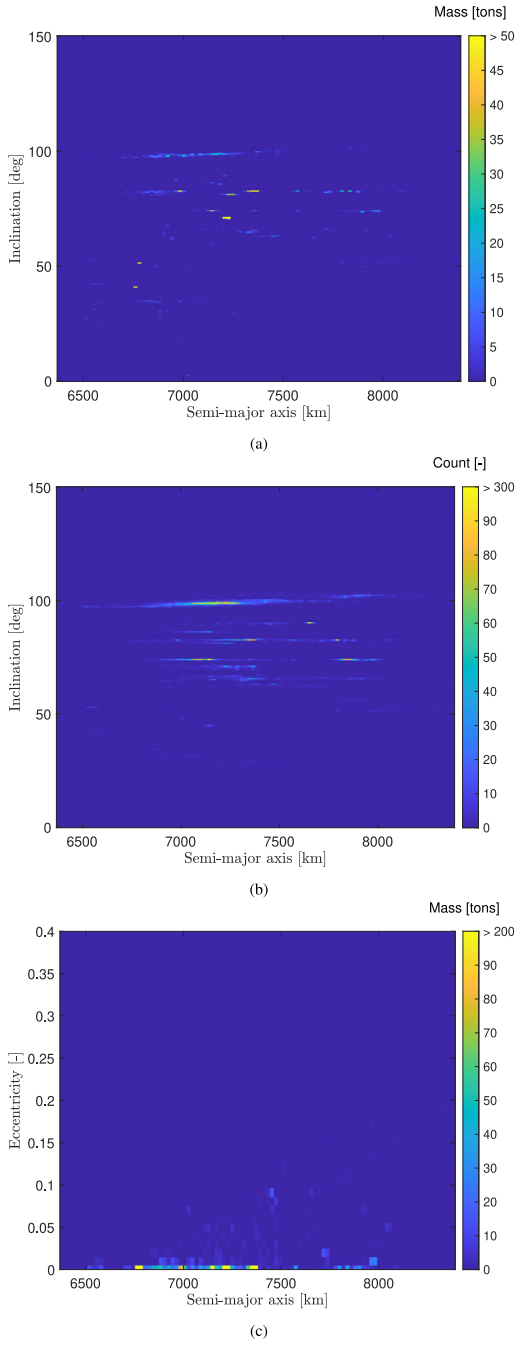

Fig. 1. (a) Mass distribution of debris objects in LEO in function of semi-major axis and inclination. (b) Number of debris objects distribution in the semi-major and inclination within the LEO region. (c) Mass distribution of debris objects in LEO in function of semi-major axis and eccentricity.

rately measuring a debris object's rotational state from the ground is extremely challenging. Various methods utilizing ground sensors have been explored and implemented in recent years, where the analysis of signal periodicity and other features is correlated with the object's rotational motion. Methods with optical telescopes (Šilha et al. (2017, 2018, 2015)), radar observations (Lemmens et al. (2013)) and laser ranging observations (Kucharski et al. (2014)) are among the solutions currently studied and implemented. These approaches come with their own set of advantages and characteristics that have impacted their practical use. For satellite laser ranging to yield highly precise measurements and estimates, retroreflectors on debris surfaces are necessary, a feature lacking in the majority of current orbital debris (Kucharski et al. (2014)). The observation of the Envisat debris leveraged this method to derive a light curve through satellite laser ranging, offering estimates into the satellite's rotational period and spin axis, as described in Kucharski et al. (2014) and Sagnières and Sharf (2019). Additionally, passive radar techniques have been employed to observe Envisat rotation, described in Lemmens et al. (2013), taking advantage of its large scale dimensions. However, it's important to note that the use of radar techniques is constrained by the inherent spatial resolution achievable for debris objects from ground-based observations. Optical techniques have been the most widely used to obtain light curve of in-space objects and estimating their apparent rotational period, as explained in the following references Vananti et al. (2021, 2018, 2020a). In this paper, information on the rotational state of debris objects is obtained from the light curve database of the Mini-MegaTORTORA (MMT-9) optical telescope MMT Telescope Light Curves (2020). To the authors' knowledge, this database is the largest publicly available source of light curve data. However, the main limitation is that data for objects with the CIS (Russia) country code is not publicly accessible.

In this database the light curves of over 12000 objects are publicly available, of which 2792 are classified as inactive objects as of August 2024. Based on the analysis of the Fourier components of the light curve, the database classifies objects according to their rotational state. The objects are categorized as *periodic*, *a-periodic*, or *non-variable*. The periodic state is given to objects which show a fundamental period of variability within their light curves acquired. The non-variable classification is assigned to objects whose light curves show no variation over time, indicating a likely stable attitude configuration. Conversely, the aperiodic objects are the objects which show a variation of the light curve, either within one track or across multiple tracks, but no periodicity of this variation can be asserted. An example of the light curve of an aperiodic object is provided in Fig. 2, while a periodic example is displayed in Fig. 3, with an apparent period of 121 s.

In Fig. 4 the statistics for the number of inactive objects observed as periodic, aperiodic, or non-variable within the dataset are reported. The small mass class includes satellites weighing 100 kg or less, the medium class covers those between 100 kg and 1000 kg, and the large class comprises objects over 1000 kg. It is important to note that the number of inactive objects with available mass data in DISCOS observed in the MMT database is 2049 out of a total of 2792. The remaining objects represent fragmentation debris for which light curve data has been collected, but no mass estimate is available. Here no specific tendency is noticeable, aside of a larger percentage of large objects showing

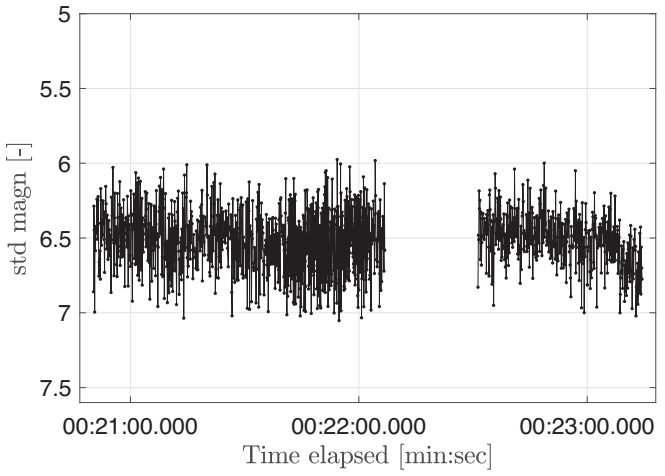

Fig. 2. Light curve obtained at epoch 12–07-2023 00:20:30 from the 25964 GLOBALSTAR M061/ GLOB object, taken from the MMT light curve database MMT Telescope Light Curves (2020).

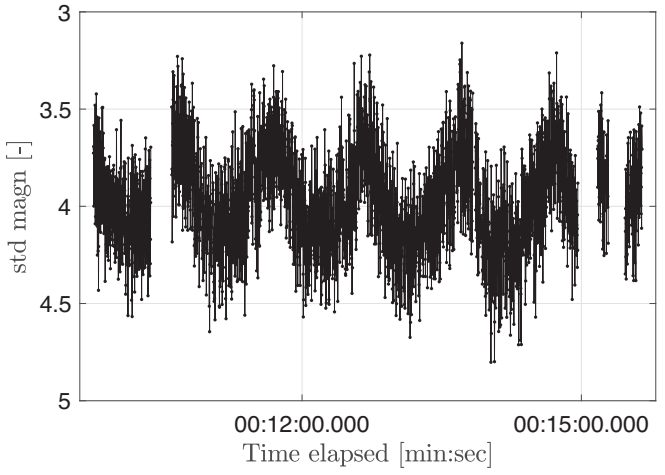

Fig. 3. Light curve obtained at epoch 12–07-2023 00:09:45 from the 32379 ATLAS 5 CENTAUR R/B/ US object, showing a period of 121 s. Data taken from the MMT light curve database MMT Telescope Light Curves (2020).

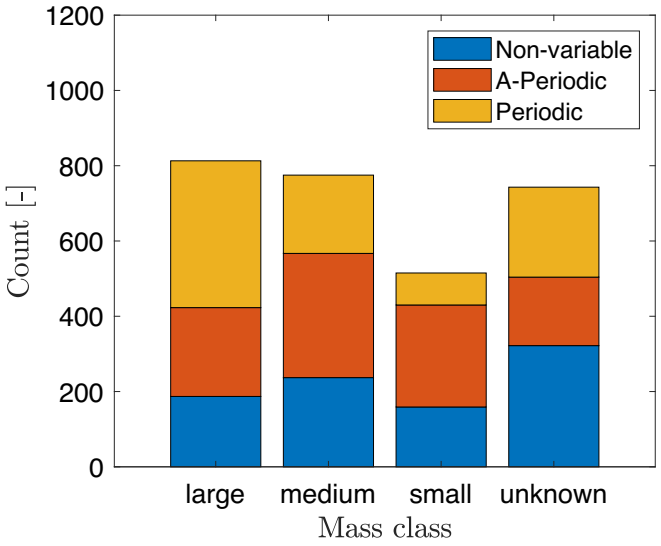

Fig. 4. Histogram of the number of stable and rotating objects divided by their mass class, observed with the MMT telescope MMT Telescope Light Curves (2020).

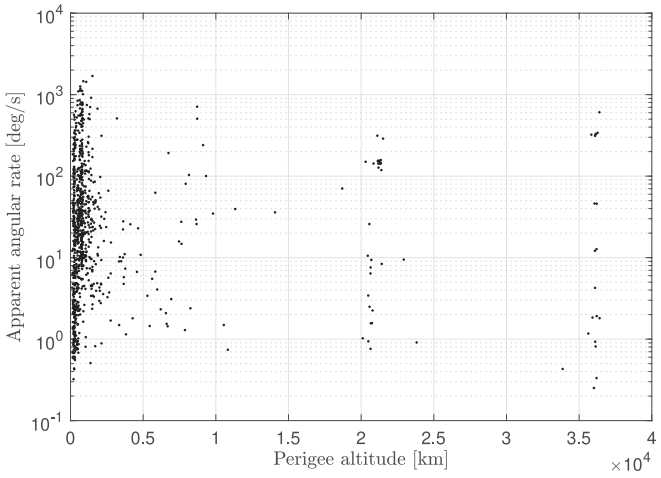

Fig. 5. Scatter plot of the objects' angular rates observed with the MMT telescope MMT Telescope Light Curves (2020) in function of their perigee altitude.

periodic behaviour. Fig. 5 displays the recorded angular rates for inactive periodic objects in the MMT database as a function of perigee altitude. It is evident that at any perigee altitude both fast and slow rotators can be present. Fig. 6 displays the distributions of perigee altitude for the rotators (periodic) and non-rotators (aperiodic and non-variable). No clear trend can be noticed from the distribution, where both rotators and non-rotators share of the total are detected at lower altitudes where atmospheric drag and magnetic field effects may dissipate the residual angular rates.

This analysis of the debris' orbital distribution and its physical and dynamical characteristics highlights the motivation for conducting a more in-depth classification of the debris using specific indices before employing the data within the multiple-target mission design framework.

3. Active debris removal index

This paper introduces the ADR index to jointly account for the various impacts that selecting specific debris targets may have on an ADR mission. Three factors are considered: (1) environmental impact, assessing the benefit to the debris environment of removing a specific object; (2) economic impact, quantifying the commercial value of removing a potential threat from a particular region; and (3) operational impact, measuring the challenges in approaching and capturing an object based on its properties and state. By combining these impacts into quantitative indices, the ADR index is defined as a weighted sum of these contributions as follows:

$$I_{\mathrm{ADR}} = w_{\mathrm{env}} I_{\mathrm{env}} + w_{\mathrm{E}} I_{\mathrm{E}} + w_{\mathrm{op}} I_{\mathrm{op}} \tag{1}$$

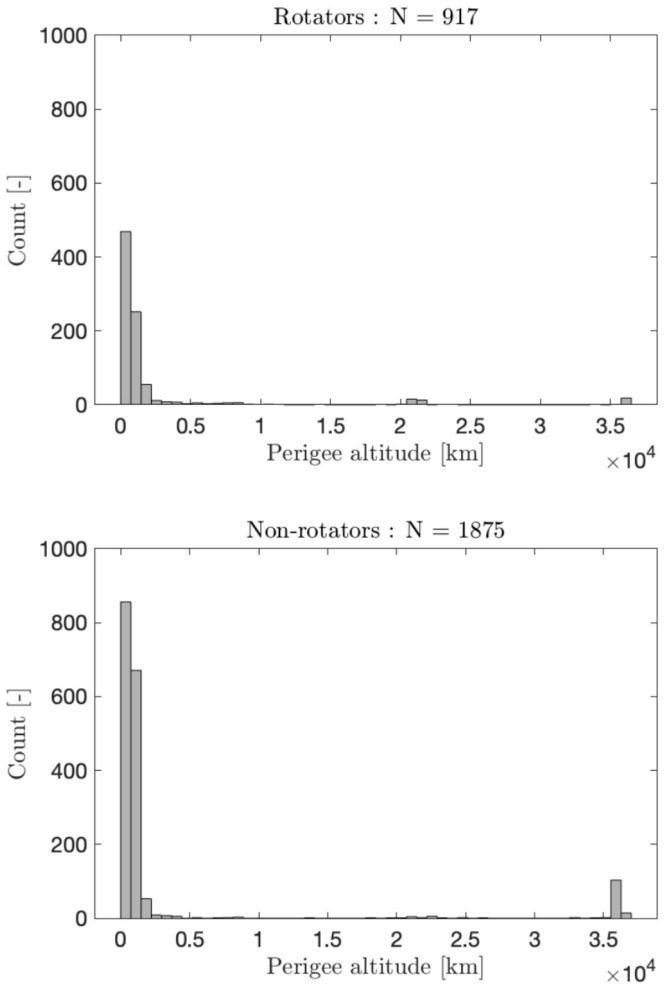

Fig. 6. Distributions of perigee altitudes of the rotators and non-rotators of inactive objects present in the MMT database MMT Telescope Light Curves (2020).

where I_{env} is the envirnomental index, and w_{env} its associated weight; I_E is the economical index and w_E its associated weight; and finally, I_{op} is the operability index and w_{op} its associated weight. The particular definition is formulated under the assumption that the impact factors are independent of one another, and the weights are intended to serve as adjustable parameters for the mission analyst to modify the relative importance of the different factors as desired. This framework is developed to classify the debris objects according to their different characteristics and is aimed at providing a tool to select the appropriate candidate and mission architecture for active debris removal. In fact, multiple ADR and mission are proven to be economically viable Braun et al. (2014, 2023), but the target selection and sequence that minimize the cost and maximize the output is a topic of research and debate which still lacks of a systematic approach. The present framework describes and classifies the debris environment to enable a meditated choice according to the different objects properties. It is important to highlight that the sub-indices, thus the ADR index, are formulated and selected to establish a ranking system that is relative in nature. This implies that achieving accurate modelling of all factors influencing an ADR mission is beyond the scope, and simpler models are often utilized instead to prioritize computational efficiency. Moreover, since the aim of the classification through these impact factors is to establish their relative significance with respect to one another, the normalization of these quantities plays a key role in defining the sub-indices and will be discussed in the following sections describing their formulation. The sub-indeces are normalised to be within the same numerical range, and the weights are intended to be tuned by the mission designer according to its prioritization criteria.

3.1. Environmental index

As previously mentioned, the environmental index describes the criticality of a particular inactive object to the orbital debris environment and is closely related to the benefits gained from its removal. In literature, different studies are present to quantify the environmental impact of a specific debris object. In 2009, Liou and Johnson presented a ranking method evaluating the product of mass and collision probability of objects from spatial densities and relative velocities (Liou and Johnson, 2009). In Yasaka (2011), the objects are studied considering their capability of generating fragments due to a collision. In the works of Anselmo and Pardini, the ranking proposed is based on the product of the probability of catastrophic collision with the number of fragments generated (Anselmo and Pardini, 2015; Anselmo and Pardini, 2016; Anselmo and Pardini, 2017). Similarly, Rossi et al. formulated the Criticality of Spacecraft Index (CSI) considering the spatial density of debris, orbital life time, mass and inclination factor (Rossi et al., 2015b). Virgili ranked the objects considering Monte-Carlo runs and evaluating the objects which are involved in collisions using long-term propagation of the debris environment (Virgili and Krag, 2013a; Virgili and Krag, 2013b). InLetizia et al. (2016), an index (ECOB) is defined based on the effects of a fragmentation, simulating its evolution and the evaluating the collision probability for a set of representative targets in the LEO region of interest. Later in Letizia et al. (2017) the ECOB index was extended to consider also the estimation of the fragmentation risks and explosions effects. Colombo et al. (2023) developed THEMIS, a index to quantitatively assess the impact of a space mission in the in-orbit environment. The work of McKnight et al. (2021) provides a comprehensive study on the methods used globally to assess high risk objects, identifying the 50 most-concerning debris to be removed.

The environmental index I_{env} used in this work is based on the previous heritage, particularly on the work of Anselmo et al. (Anselmo and Pardini, 2015; Anselmo and Pardini, 2016; Anselmo and Pardini, 2017). The choice was made considering the trade-off in complexity and computational expense in the evaluation with the proper mod-

elling of the environmental effect of a debris. Specifically, the index represents a quantification of the probability of collision of an object P_c and the number of fragments generated in its breakup N_f. The formulation of Anselmo and Pardini (2016) is reported in the following equations.

$$P_c \approx \Phi \cdot M \cdot life(h) \tag{2}$$

$$N_f \approx M^{0.75} \tag{3}$$

$$I_{env} = \left(\frac{\Phi}{\Phi_0}\right) \cdot \left(\frac{M}{M_0}\right)^{1.75} \cdot \left(\frac{\mathscr{L}}{\mathscr{L}_0}\right) \tag{4}$$

In Eq. 2, Φ is the current debris flux encountered by the object, M is the mass of the object from DISCOS database and $\mathscr{L}$ is the orbital lifetime function. In this work, Φ is computed using the MASTER-8 environment model (Braun et al., 2021), considering objects with size greater than 10 cm. The size threshold selected corresponds to a catastrophic collision with impact energy of 40 J/g in LEO as indicated in reference Oikonomidou et al. (2021). Only catastrophic collision risks are considered in this definition to reflect the impact that a fragmentation of the object will have on the space environment over the long term. For computational purposes, the flux is computed for a 2D grid in mean altitude and inclination in LEO, shown in Fig. 7, and the specific value for each LEO object is obtained through simple interpolation. The mean altitude is defined subtracting the mean Earth's equatorial radius to the semi-major axis. Mean altitude results equivalent to the constant altitude only in the case of a circular orbit. The orbital life time function is computed using the semi-analytical propagator PlanODyn developed at Politecnico di Milano (Colombo, 2016). A cut-off in reentry time of 200 years is set to avoid excessive weighting of high altitude objects. Eq. 3 expresses the number of fragments generated from a catastrophic collision according to the NASA break-up model in adherence with (Johnson et al., 2001). The environmental index of Eq. 3 is then normalized with the value corresponding to an object of 1000 kg of mass in an orbit of 800 km of altitude and 98.5 deg of inclination. The present definition results in higher values of environmental index for objects which pose an higher risk to the debris environment.

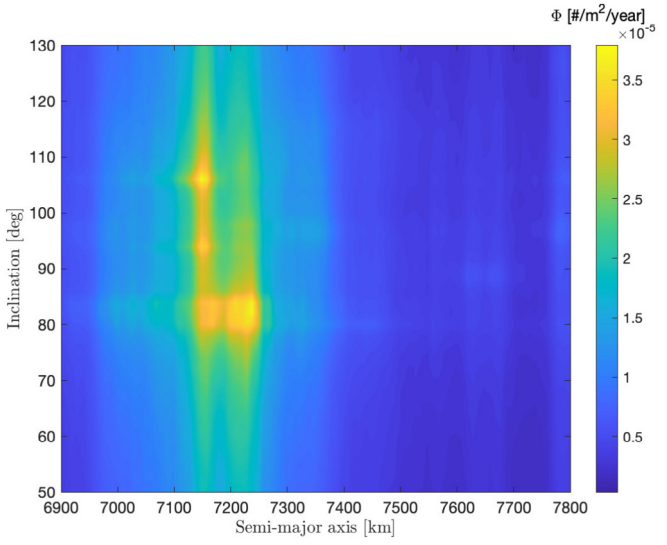

Fig. 7. Debris flux grid in LEO computed with the MASTER-8 model considering objects greater than 10 cm.

3.2. Economical index

The previously defined environmental index considers the criticality of each object's presence in the near-Earth environment, primarily focusing on the long-term risk of collisions and their potential impact on space operations. However, this approach does not fully address the economic implications of debris removal, particularly in terms of safeguarding space resources that are valuable for commercial exploitation. While the environmental index assesses collision risks and their effects over time, it does not factor in the potential threat that specific debris objects pose to the economic value of the orbital regions they occupy.

To complement this evaluation, we introduce a metric that quantifies the economic and commercial risk posed by space debris. This metric assigns a value, referred to as the economic index I_E, to each altitude and inclination bin, reflecting the potential economic resource value endangered by the presence of debris in those specific orbital regions. By incorporating this economic perspective, we aim to quantify the advantages debris removal efforts that not only mitigate collision risks but also protect the commercial viability of key orbital zones.

In the literature, various studies have been conducted to model and evaluate the economic value of orbital resources, both from the perspective of assessing commercial losses due to orbital debris risks Adilov et al. (2023) and of estimating a satellite tax to compensate for these risks Rao et al. (2020); Macauley (2015); Béal et al. (2020). In the work of Adilov et al. (2023) the value of an orbital asset is modelled according to functions of its mass, using a constant cost per kilogram model and a fitting model retrieved by real insurance data of past satellites Kunstadter (2021).

The model used in this work to define the value of an orbital slot is based on the one introduced in the work of Colombo et al. (2017), where a the active satellite types and mass of the orbital regions are used as a proxy for the economical value of the them. To relatively weight the value of the different satellite types, the revenues value of the space economy from the Satellite Industry Association (SIA) report of 2023 are used, which define the different value of each services provided by active satellites in orbit. In this report, the global value of the space economy is studied and revenue streams of different satellite applications are quantified. From a mathematical perspective, the economical index of an orbital slot $(\Delta a, \Delta i))$ is defined as:

$$\bar{I}_{\mathrm{E}} = \sum_{k} \sum_{j \in (\Delta a, \Delta i)} \left(M_j Q_{k,j}\right) \frac{1}{Q_{tot}} \frac{1}{M_{k,tot}} \tag{5}$$

$$I_{\mathrm{E}} = 3 \log \left(\frac{\bar{I}_{\mathrm{E}}}{\bar{I}_{\mathrm{E0}}} \right) + 30 \tag{6}$$

In Eq. 6, $Q_{k,j}$ is the estimated revenue value of the satellite k-th revenue categories assigned to the satellite j, while M_j represents its mass. $M_{k,tot}$ and Q_{tot} are respectively the total mass of satellites of the k-th type and the total revenue value of the satellite industry. The satellites types have been retrieved from the UCS satellite database, which comprehend 30 different types, among which are for example Earth observation, communication, navigation, Earth science etc. These types are mapped to the revenue categories of satellite services taken from the SIA 2023 report, which include telecommunication, governmental space budgets and institutional, remote sensing. The discretisation bins widths are considered 50 km and 0.25 deg in altitude and inclination respectively. Again, the I_{E} index is normalised with the value computed for the SSO bin of 800 km of altitude and 98.5 deg of inclination and defined in a logarithmic scale, as reported in Eq. 6, to guarantee a comparable interval between maximum and minimum values and a meaningful comparison in the aggregation with the other sub-indeces in the ADR index. Indeed, a more advanced assessment of satellite value based on specific mission characteristics (e.g., resolution, coverage, operating frequencies and downstream supported services) could improve the accuracy of orbital slot valuation. However, such data are often not publicly available for all current missions and are difficult to obtain. Therefore, the simplicity of our model is also constrained by the availability of open-source data. The computed map in mean altitude and inclination with the first model of economical resource value of the LEO orbital region is shown in Fig. 8. A debris objects is then assigned an economical index according to the orbital slot value computed in the semi-major axis and inclination grid.

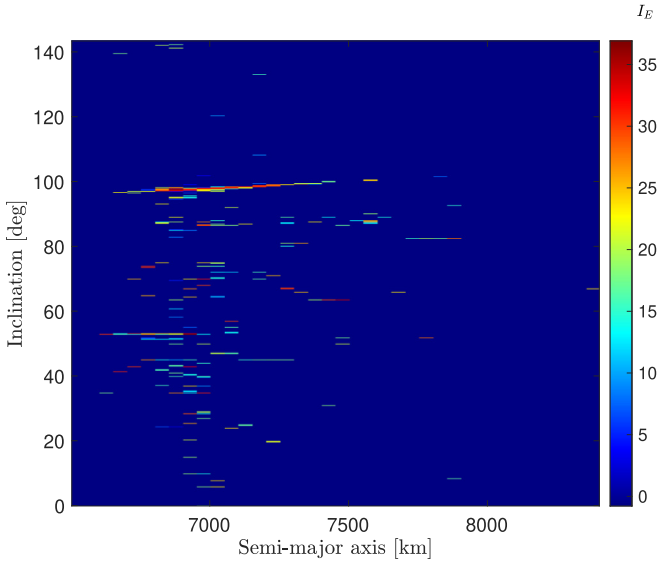

Fig. 8. Map of the economical index displayed for the altitude and inclination bin defined in the LEO region.

3.3. Operability index

The last contribution to the ADR index of Eq. 1 is introduce to describe the feasibility and complications arising during the operations of approach and capture of a debris object in the context of an ADR mission. Despite the significant efforts devoted to advancing and addressing the technical challenges of debris capture and removal, a high-level assessment of each object's suitability for capture based on its state and characteristics is, to the authors' knowledge, not yet available in the literature. Specifically, the operability index I_{op} aims to quantify the difficulties in the approach and capture of an uncooperative target based on its physical and dynamical characteristics. Three main properties of the target are considered to influence the approach and capture phases:

- **Attitude state**: The tumbling motion of the target will require the servicer to synchronise to its motion in order to rigidly attach to the target.
- **Mass**: A massive satellite will impose more stringent constraints on the capture mechanisms employed and propellant requirements for the deorbiting.
- **Illumination conditions**: Relative sensors measurements and operations are poorly affected by difficult illumination conditions, i.e. eclipse regions.

The definition of current impact factors relies on the assumption of a rigid capture method, such as robotic arms, with the consideration that the maturity level for future implementation is higher than that of flexible methods, such as tether nets. If one considers alternative capture methods, some of the latter considerations may become inapplicable, while some may be added.

The information regarding the attitude state of each debris object is taken considering the light curve data as described in Section 2, where the apparent period and rotational state is retrieved. Despite the apparent period does not represent directly the target absolute angular rate, it provides an estimation of the entity and scale of a debris attitude state. A more accurate estimation of the target shape and attitude motion based on light curve data is also a active field of research, as described in (Allworth et al., 2020b; Blacketer et al., 2019). However, such high fidelity estimation is out of the scope of this study which mainly aims to rank and weight the debris population according to its characteristics in a relative fashion. The choice of the light curves as a proxy representation of the target attitude motion can be further motivated by the work of Sagnières and Sharf (2019) and Silha et al. (2017), where the light curves of Envisat was studied over time in comparison with simulation based and higher fidelity data acquired (through radar and satellite laser ranging meth-

ods). One major drawback for the fidelity of using this data is the not complete availability for all objects. However, no other means of reliably estimate the attitude state of an inactive objects has been identified in this study. It should be noted that complementing this data availability will improve the operability index representativeness.

The operability index is defined as the product of various factors that quantify these considerations, with its value designed to be directly proportional to the feasibility and ease of approaching and capturing a target.The proposed formulation is as follows:

$$I_{\text{op}} = P_{\text{ill}} S_f \mathscr{A}(\omega, L, \omega_0, L_0) \left(\frac{M_0 - M}{M_0} \right) \tag{7}$$

which depends on the illumination factor P_{ill}, the shape factor S_f, an acceleration function $\mathscr{A}(\omega, L, \omega_0, L_0)$ and the mass of the debris object M. The term P_{ill} represents the average percentage of orbit in eclipse during a one year simulation, estimating the probability for each object to encounter a poor illumination condition during the approach rendezvous and capture. It is worth noticing that poor illumination conditions do not prevent the successful completion of capture, since the proximity operations can be planned in time accordingly or specific sensors can be employed which overcome this difficulties. However, it will impose additional constraints from the mission analysis and system design point of view which can be of relevant influence in the mission design process. The term S_f in Eq. 7 represents a shape factor between 0 and 2 classifying complex shapes to be captured from the shapes property contained in the DISCOS database. Table 1 shows some example of shapes in the classification performed, together with the associated shape factor S_f considered.

The acceleration function introduced in the index definition of Eq. 7 aims to represent the acceleration level required to synchronise with the target object rotational motion to achieve rigid capture. The acceleration level will depend on the rotational state of the target, together with the safe distance of approach during proximity operations and capture. The definition is based upon the compensation centripetal relative acceleration needed by the chaser satellite to synchronise with the target rotational motion, which is expressed as $L\omega^2$ where L is the safety distance and ω is the target's angular rate. The expression of the acceleration function is as follows:

Table 1
Debris objects shape classification.

Easy	Moderate	Hard	Very hard
$S_f = 2$	$S_f = 1$	$S_f = 0.2$	$S_f = 0$
Box	Box + 1 panel	Box + 2 panel	Box + 1 sail
Box + Cyl	Box + 1 dish	Box + 2 arms	Box + 1 tether
Cone	Box + 1 rod	Box + 4 ant	Cone + 1 sail
Cyl	Cyl + 2 dish	Box + 6 panel	Box + 1 ant + 1 sail
Sphere	Box + 1 truss	Cyl + 4 panel	Box + Box + tether
...	...	...	...

$$\mathscr{A}(\omega, L, \omega_0, L_0) = \begin{cases} 2 - \frac{L\omega^2}{L_0\omega_0^2} & \text{if} \quad \omega \leqslant \omega_0 \\ \frac{L_0\omega_0^2}{L\omega^2} & \text{if} \quad \omega > \omega_0 \end{cases} \tag{8}$$

The function $\mathscr{A}(\omega, L, \omega_0, L_0)$ is defined as a monotonically decreasing function, which models the decreasing feasibility of synchronisation and capture at growing angular rates. The piecewise definition is leveraged to guarantee a linear trend for angular rates less than the ω_0 value, which is set to 3 deg/s a value that considers the feasibility of capture in past studies Nishida and Kawamoto (2011). This is introduced to avoid excessive weighting of slow rotators using the reciprocal relationship used for values of angular rates greater than 3 deg/s. Instead of introducing a cut-off value at the threshold angular rates studied in literature Nishida and Kawamoto (2011), the monotonic increase is maintaned considering that technologies such as tentacle like robot arms Biesbroek et al. (2021) or detumbling of the target prior capture Peters and Olmos (2016, 2024) can be used, although introducing complexities in the propellant expenditure, servicer design and synchronisation requirements. For the objects which do not show in the light curve data any periodicity, labelled as aperiodic and non-variable, a constant angular rate equal to the orbital mean motion $\omega_a = n$ deg/s is taken. This assumption is based on the idea that if no variation in the reflected light along the sensor's line of sight is detected, the apparent rotation in that direction can, at most, correspond to the object's orbital revolution rate around Earth. The safe distance L is defined from the largest dimension of each object taken from the DISCOS database, while the baseline L_0 is taken equal to 2 meters.

Finally, a mass dependency is introduced as a simple linear inverse proportionality weighting the largest masses as the harder to be captured, stabilised and deorbited. A normalisation with a mass M_0 equal to 10 tons in Eq. 7 is considered.

4. Debris ranking in low Earth orbit

The proposed ranking framework based on the ADR index I_{ADR} metric is here applied to candidate debris objects in LEO. The objects analysed are the one with mass greater than 100 kg and in the mean altitude region between 400 km and 2000 km, e.g., the LEO protected region ESA Space Debris Office (2024).

In order to properly scale the different contributions relative to each other, the weights in Eq. 1 are considered as follows: $w_{\text{env}} = 1, w_{\text{E}} = 1$, and $w_{\text{op}} = 10$. The peculiar choices are dictated both by the relative importance given to the different sub-indices in the context of a general debris remediation mission, and from the fidelity of the employed model for the assessment. This choice allows the ranges of minimum and maximum of the single sub-indeces to be comparable, and therefore provide an example of how the different aspect influence different objects in the population. In the cases where the ADR service is designed to

specific needs or with specific priorities, the weights should be adjusted accordingly. An example is the case of a commercial ADR service provided to satellite operators, where the remediation and reduction of collision risk and avoidance manoeuvres frequency and long-term risk in the orbital region of more economical resource values may be prioritized, thus the weight of the economical index would increase with respect to the others.

Table 2 reports the top 50 ranked objects obtained from the index example application to the analysed population. It can be noted the first spots are mostly taken from large rocket bodies in the SSO region and in the 70 deg of inclination region. These are characterised mainly by a large environmental index, driven by the large debris flux experienced in that regions and the large mass, which will introduce more fragments in the case of a catastrophic collision.

Table 2
Generated ranking of the first 50 objects identified by the ADR index in LEO.

NORAD	Type	Name	Mass [kg]	sma [km]	i [deg]	I_{env} [–]	I_{op} [–]	I_E [–]	I_{ADR} [–]
28353	RB	Zenit-2 s stage	9000	7222	71.00	49.85	0.01	25.03	75.03
31793	RB	Zenit-2 s stage	9000	7222	70.97	49.65	0.02	25.03	74.83
26070	RB	Zenit-2 s stage	9000	7218	71.00	48.83	0.01	25.03	74
27386	PL	Envisat	8110	7141	98.29	46.69	0.27	22.14	71.51
22566	RB	Zenit-2 s stage	8500	7220	71.01	44.57	0.02	25.03	69.84
25400	RB	Zenit-2 s stage	8226	7184	98.75	39.04	0.03	30.36	69.65
23088	RB	Zenit-2 s stage	8226	7221	71.00	42.28	0.03	25.03	67.6
20625	RB	Zenit-2 s stage	8226	7221	71.00	42.29	0.02	25.03	67.57
23705	RB	Zenit-2 s stage	8226	7219	71.02	41.95	0.03	25.03	67.24
23405	RB	Zenit-2 s stage	8226	7219	70.98	41.89	0.02	25.03	67.16
19650	RB	Zenit-2 s stage	8226	7217	71.00	41.62	0.03	25.03	66.92
25407	RB	Zenit-2 s stage	8226	7217	71.01	41.62	0.02	25.03	66.89
16182	RB	Zenit-2 s stage	8226	7216	71.00	41.52	0.02	25.03	66.79
22220	RB	Zenit-2 s stage	8226	7215	71.00	41.46	0.03	25.03	66.77
17590	RB	Zenit-2 s stage	8226	7214	71.00	41.39	0.03	25.03	66.7
22803	RB	Zenit-2 s stage	8226	7213	70.99	41.37	0.03	25.03	66.68
17974	RB	Zenit-2 s stage	8226	7212	71.01	41.29	0.02	25.03	66.57
19120	RB	Zenit-2 s stage	8226	7205	71.01	40.57	0.02	25.03	65.85
23752	PL	Skipper	228	7183	98.82	0.07	3.2	30.36	62.46
48607	RMRO	Starlink operational debris	100	6936	53.03	1.4e-3	2.54	36.91	62.26
24753	PL	DMSP Block 5D-2 F14	816	7216	98.86	0.75	3.22	28.69	61.67
28891	PL	Topsat	115	7061	98.22	3.1e-3	2.78	32.9	60.73
6276	RB	Star 26B (Thor-Burner IIA)	115	7198	98.54	0.02	3.05	30	60.55
1430	PL	Tiros X	126	7133	98.44	0.03	2.9	30.93	60.01
6788	RB	Star 26B (Thor-Burner IIA)	115	7181	98.72	0.02	2.96	30.36	59.94
56229	PL	Skykraft 3 Carrier	100	6867	97.55	9,3e.4	2.48	34.74	59.58
28368	PL	Demeter	132	7010	98.04	3.7e-3	2.63	33.26	59.56
7817	RB	Star 26B (Thor-Burner IIA)	115	7205	98.74	0.02	3.06	28.69	59.32
43644	RMRO	YG-32 Adapter	200	7052	98.01	2.6e-3	2.6	33.26	59.26
26103	RB	PEGASUS-2 (Taurus)	223	6873	97.39	3.0e-4	2.45	34.74	59.23
23533	PL	DMSP Block 5D-2 F13	1487	7215	98.82	2.16	2.84	28.69	59.22
4954	RB	Star 37B (Thor-Burner II)	154	7140	98.41	0.03	2.8	30.93	58.97
4953	PL	DMSP 5A-F6	416	7132	98.58	0.22	2.78	30.93	58.91
4047	PL	DMSP 5A-F3	416	7173	98.51	0.23	2.86	30	58.83
44887	RMRO	CZ-4B operational debris	200	6985	97.84	9.3e-4	2.54	33.37	58.82
3522	RB	Star 37B (Thor-Burner II)	154	7169	98.72	0.04	2.83	30.36	58.74
3510	PL	DMSP 5A-F2	416	7177	98.49	0.22	2.84	30	58.63
7412	RB	Star 26B (Thor-Burner IIA)	115	7192	98.64	0.02	2.81	30.36	58.51
23324	RB	PSLV fourth stage (PS4)	912	7213	98.93	0.91	2.99	27.68	58.5
28637	RB	ORION 38	410	7231	98.74	0.23	2.96	28.69	58.49
6218	RB	Star 37B (Atlas F)	154	7084	98.59	0.01	3.05	27.68	58.21
27945	PL	KAISTSat-1	106	7050	98.30	3.9e-3	2.75	30.71	58.19
49385	RMRO	Yaogan Weixing 32 adapter	200	7050	98.20	2.5e-3	2.72	30.71	57.88
28898	RB	Cosmos 3 s stage	1569	7063	98.26	0.79	2.4	32.9	57.73
37390	RB	PSLV fourth stage (PS4)	920	7177	98.41	0.87	2.66	30	57.49
12553	PL	NOAA 7	717	7212	98.89	0.58	2.92	27.68	57.46
27422	RB	H10 (Ariane 42P H10)	1820	7169	98.53	2.87	2.46	30	57.43
20443	RB	H10 (Ariane 40 H10)	1764	7140	98.39	2.01	2.45	30.93	57.4
41039	RB	L-14B-res (YF40B-res)	1000	6891	97.57	2.9e-3	2.26	34.74	57.37
54362	RB	PSLV fourth stage	960	6861	97.46	4.5e-3	2.26	34.74	57.37

However, these objects do not possess a high operability index. Furthermore, high position in the ranking is occupied by the ESA owned Envisat, which have been studied as a target for a ADR missions in the past (Biesbroek et al., 2017). It is interesting to note how in the generated ranking there are less massive objects which are not characterised by a large environmental index, but they score well in terms of operability index and economical index. For example operational debris of the Starlink constellation at 53 deg of inclination which is stable as rotational motion and has high operability index, or also some smaller objects in Sun-Synchronous region, i.e. Skipper payload and Star 26B (Thor-Burner IIA) stages. Interestingly, the particular ranking using the example weight proposed in Table 2 shows similar results in the top positions with the ranking presented in the work of McKnight et al. (2021). Particularly, the Zenit-2 stages dominate the first positions, showing combined high scores both in the environmental impact (captured also by McKnight et al. (2021)) and economical index. Notably, a difference is the placement in the ranking of Table 2 of objects which have combined large operability and economical index with respect to McKnight top 50, in which these impacts were not considered explicitly.

These first 50 ranked objects are also displayed in the altitude and inclination plot in Fig. 9, where each object's circle radius is proportional to the objects' mass and the colormap display the MASTER-8 objects flux considered in Section 3.1. As pointed out from Table 2, they are evident the two clusters dominating the ranking in SSO and aroud 70 deg of inclination and 800–900 km of mean altitude.

Fig. 10 shows the scatter distribution of the environmental index I_{env} and economical index I_{E} for the population analysed. At first glance, it can be noted that some debris score medium to high on the environmental index but are close to zero on the economic index, indicating no commercial interest in their removal from this orbital region. Some

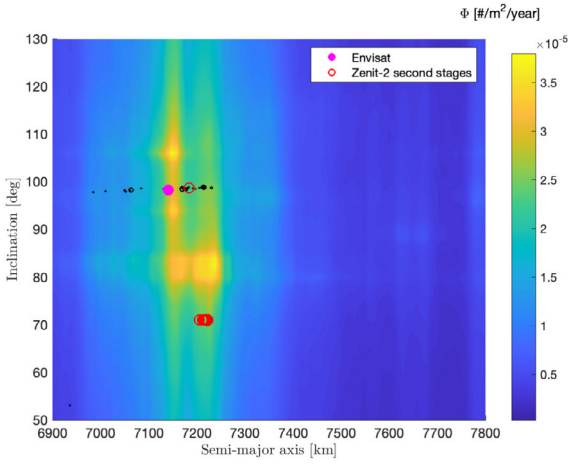

Fig. 9. Scatter plot of the first 50 ranked objects according to the ADR index super-imposed to the in-orbit debris flux computed from MASTER-8 (Braun et al., 2021).

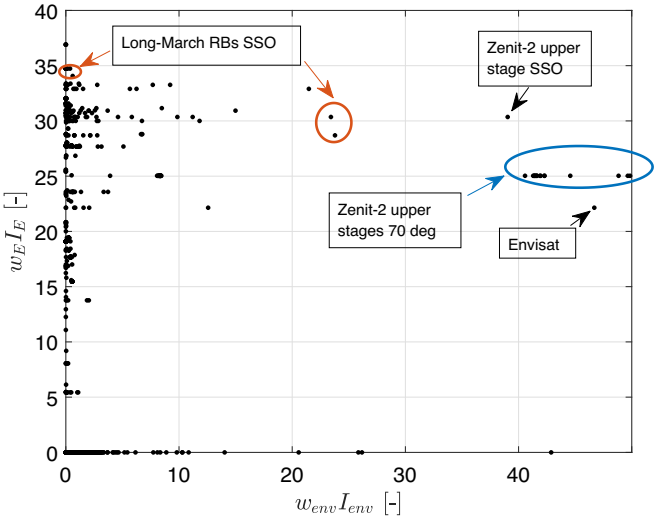

Fig. 10. Scatter distribution of the debris objects in LEO in function of their environmental index I_{env} and economical index I_{E}, with some notable objects highlighted. Note that both indices have been multiplied by their associated weights.

objects are also present which have the highest combined score in the distribution plot shown in Fig. 10, i.e. Envisat and other objects in SSO. The distribution of the objects in the envirnomental index and operability index domain is displayed in Fig. 11. Notably, two distinct block are evident, representing objects with high and low operability among the overall population. Within these blocks, a wide range of environmental index is observed. The distribution of these properties is influenced by the angular rate conditions of the debris, leading to the stacking of stable objects in the block with higher operability index values. It is also noteworthy that a greater number of object is present in the block of low operability, representing conditions of complex shapes, large angular rates, and large mass.

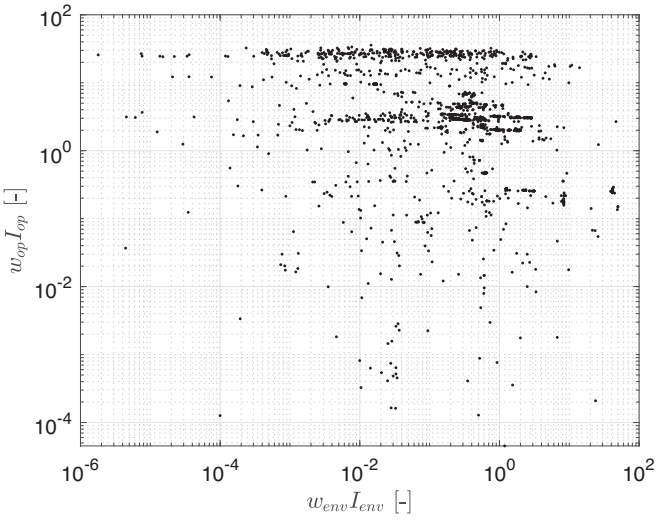

Fig. 11. Scatter distribution of the debris objects in LEO in function of their environmental index I_{env} and operability index I_{op}. Note that both indices have been multiplied by their associated weights.

5. Multiple target removal design tool

The previously described index formulation is employed in this work in a multiple ADR mission design tool to optimally select the target sequence. The goal of the tool is to provide mission analysts with a flexible tool for preliminary planning of multi-target ADR missions, which can be tailored to specific needs using the index definition. The design tool is used to select the optimal removal sequence to maximize impact while minimizing mission costs. The mission design problem addressed in this paper assumes a chaser + kits mission architecture and considers impulsive transfers to a fixed number of debris targets.

5.1. Mission architecture

Various mission architectures for debris removal, specifically for multiple targets, have been explored in the literature. The simplest and most straightforward solution for a multiple ADR mission involves a single monolithic satellite servicer that sequentially rendezvouses with and captures each target, performing a disposal orbit injection before moving on to the next target. In this approach, the servicer's propulsion system is used to transfer both the servicer and the debris to disposal orbits, after which the servicer detaches and proceeds to the next target's orbit. Disposal orbits are typically selected to ensure a faster reentry of debris towards Earth, which would not happen in the current situation. While this mission architecture is conceptually simple, it has the drawback of high mission costs in terms of propellant, as the servicer must transport both itself and the debris to and from disposal orbits. This generally limits the number of objects that can be removed by a single servicer due to propellant constraints.

Another mission architecture explored in Huang et al. (2020) leverages an orbiting station placed in a convenient orbit to serve as a refueling platform for the servicer during the removal process. While this option introduces greater complexity in terms of mission design and cost—since the station itself must be designed, launched, and maintained—it increases the servicer's capacity to remove more targets within the same mission. Lastly, a mission architecture utilizing removal kits has also been explored in the literature. In this approach, the servicer carries multiple removal kits as payloads. These kits, equipped with their own propulsion systems, are attached to each debris object. This allows the deorbiting burns to be handled by the kit alone, avoiding the need to expend servicer propellant to transport both the servicer and debris to and from disposal orbits as part of the capture stack (Huang et al., 2020; Colombo et al., 2021).

In this paper the deorbiting kits mission architecture is considered, which concept is displayed in Fig. 12. Chemical propulsion is assumed for both servicer and removal kits, assuming a specific impulse of 250 s.

The mission design is focused on the computation of the transfer delta-v and time of flight required from the *i-th* debris to the next debris of the sequence. The dynamics considered are the J_2 perturbed motion of satellites in the near Earth environment. The model dynamics can be expressed considering the mean variation of the Right Ascension of the Ascending Node (RAAN) and the argument of the perigee due to the J_2 zonal harmonic of the geopotential. Atmospheric drag effects are neglected in the orbital dynamics, as the orbits of the debris targeted by ADR are assumed to experience minimal drag influence over the mission time frame - otherwise, ADR would not be of practical interest. Other perturbations affecting LEO dynamics, such as solar radiation pressure and third-body gravitational effects, are also neglected at this stage of the study. This assumption significantly simplifies the orbital dynamics and their implementation within the mission design tool, which is intended for preliminary mission analysis and target selection. In later, more refined phases of mission design, these perturbations will need to be included to accurately model the transfer trajectories to the target orbits. Accordingly, the mean orbital elements rates can be expressed as:

$$\begin{cases} \dot{a} = 0, \quad \dot{e} = 0, \quad \dot{i} = 0 \\ \dot{\Omega} = -\frac{3}{2} J_2 \left(\frac{R_e}{a(1-e^2)} \right)^2 n \cos i \\ \dot{\omega} = -\frac{3}{4} J_2 \left(\frac{R_e}{a(1-e^2)} \right)^2 n (5\cos^2 i - 1) \end{cases} \tag{9}$$

where a is the semi-major axis, e the orbit eccentricity, i the orbit inclination, Ω the Right Ascension of the Ascending Node (RAAN) and ω the argument of the perigee of the satellite orbit. Note the elements considered are the mean elements and the dynamics is the average variation of the osculating elements across one orbital period.

The problem of mission design of multiple target removal mission can be described as the sequence of debris is to be selected such that the transfer cost is minimised. More specifically the mission design problem can be divided in a optimisation problem for each transfer nested within the combinatorial problem of selecting the sequence of targets to be removed.

5.2. Transfer strategy

Being the servicer assumed to be equipped with chemical propulsion engine, impulsive transfers strategies between an initial and target orbit are devised for the multiple ADR mission. The delta-v estimation and time of the transfer is obtained considering a sequence of simple impulsive manoeuvres to correct the difference in orbital elements between the two debris. Firstly, a Hohmann transfer is used to change the semi-major axis resulting in a delta-v cost expressed as follows:

$$\Delta V_{HT} = \sqrt{\frac{\mu}{r_1}} \left(\sqrt{\frac{2k}{1+k}} - 1 \right) + \sqrt{\frac{\mu}{k r_1}} \left(1 - \sqrt{\frac{2}{1+k}} \right) \tag{10}$$

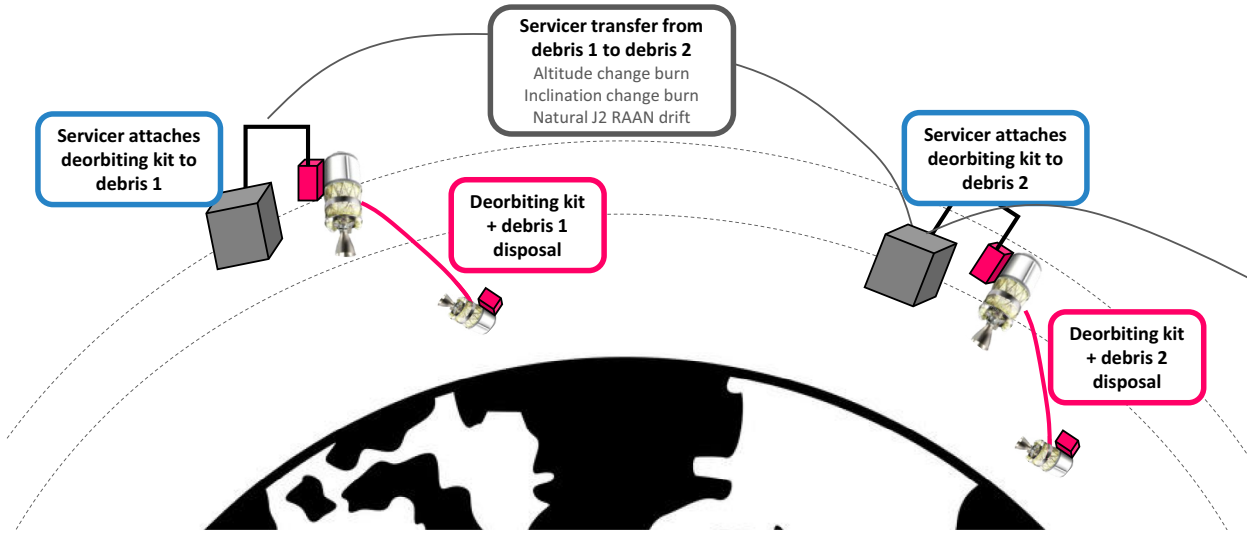

Fig. 12. Illustration of the multiple ADR mission architecture envisioning a servicer equipped with deorbiting kits which sequentially attaches them to the debris objects to deorbit them.

where k is the ratio between a_1 and a_2, semi-major axis of debris 1 and debris 2 respectively, assuming circular orbits. The difference of inclination is compensated by a plane change manoeuvre at the node which has the following delta-v cost:

$$\Delta V_{PC} = 2V_1 \sin((i_1 - i_2)/2) \tag{11}$$

Note that the assumptions of circular initial and target orbit for the transfer manoeuvres of Hohmann and plane change is used, which is reasonable according to the distribution of debris object mostly on near-circular orbits around Earth.

Moreover, the transfer strategy to move from debris 1 to debris 2 shall also compensate the RAAN difference, to match the two orbital planes. Different strategies can be used to obtain a RAAN change between two orbits:

- *Direct plane change*: a ΔV along the normal is used to directly change the plane orientation with impulsive action. The delta-v required for such manoeuvre is computed as:

$$\Delta V_{\Delta\Omega} = 2V_1 \sin((\Omega_1 - \Omega_2)/2) \tag{12}$$

- *Natural drift*: The differential change in the RAAN between the two orbits caused by the J_2 perturbation will eventually lead to a convergence to the same value (i.e., same plane). This convergence is typically reached by taking into account the waiting time required for the RAAN alignment to occur naturally expressed as follows:

$$\Delta T_{nat-J_2} = \frac{\Omega_{02} - \Omega_{01}}{\dot{\Omega}_1 - \dot{\Omega}_2} \tag{13}$$

which depends on the difference of orbits between the two debris objects. The RAAN drift rate for each orbit is computed with the mean variation from Eq. 9. This will cause large time of flight, but with the advantage of not using any delta-v for this manoeuvre.

- *Drift orbit strategy*: An intermediate drift orbit is used to enhance the RAAN drift difference due to the J_2 perturbation and reduce the time of flight to match the two orbital drifting plane. Here the strategy of changing the altitude to act on the RAAN drift rate of the drift orbit is usually employed. This will allow a limited cost of transfer to the drift orbit with respect to a change of inclination, and an enhanced effect on the achievable drift. The time of flight on the modified drift orbit is expressed as:

$$\Delta T_{drift-orb} = \frac{\Omega_{02} - \Omega_{01}}{\dot{\Omega}_{drift} - \dot{\Omega}_2} \tag{14}$$

with the RAAN rate on the drift orbit obtained by modifying the orbit semi-major axis and eccentricity as:

$$\dot{\Omega}_{drift} = -\frac{3}{2} J_2 \left(\frac{R_e}{a_{drift}\left(1 - e_{drift}^2\right)} \right)^2 n_{drift} \cos i_1 \tag{15}$$

In this research, we utilise the natural drift approach, where a waiting period described by Eq. 13 is introduced between debris object 1 and debris object 2. This waiting time is necessary to achieve a matching RAAN condition without resorting to propellant-based manoeuvres. It is worth emphasising that this choice does not represent an efficient strategy in terms of total time of flight of the overall mission. Besides considering the cost of propellant, the mission's time of flight is a significant factor in both mission design and operations. If minimising the total time of flight is as critical as reducing propellant consumption for the multiple ADR mission, alternative strategies should be explored. Another important thing

to point out is that the delta-v required to align with orbit anomalies and successfully rendezvous with the target is not taken into account at this stage. This assumption is motivated by the possibility of conducting phasing manoeuvrers along orbits with the same shape and plane after other transfer manoeuvrers and the limited allocation of propellant resources for these type of manoeuvrers. After the estimation of the cost for transferring from debris 1 to debris 2, an estimation of the delta-v needed from the deorbiting kit is required. A perigee lowering manoeuvres is assumed to be performed by the kit attached to the debris to reach perigee altitude of 400 km.

The propellant expenditure for each of the delta-v manoeuvre planned, including the deorbit burn provided by the deorbiting kit, is estimated through Tsiolkovsky equation:

$$\Delta V = I_{sp} g_0 ln\left(\frac{m_0}{m_f}\right) \tag{16}$$

where m_0 and m_f represent the initial and final mass during the burn. For delta-v transfer manoeuvrers, the initial mass consists of the platform, the remaining de-orbiting kits with their propellant, and the platform's propellant. In contrast, for the de-orbiting burn performed with the kits, the initial mass includes only the kit structure and the propellant contained within the kit. This formulation allows for the estimation of propellant mass across different delta-v burns, while ensuring that all contributions are accounted for in the total initial wet mass.

5.3. Multi-objective mission design tool

In this section the mission architecture, transfer strategies and the ADR index definitions are embedded in a multi-target mission design tool. This tool aims to optimally choose the sequence of debris to retrieve with the defined architecture which minimise specific cost metrics. Specifically, the novelty brought by this paper lies in considering, together with the usual mission cost, the ADR index presented in 3 as a cost metric for the mission design. This results in a multi-objective optimisation tool to minimise the mission cost while maximising the mission effect and feasibility, i.e. conveyed by ADR index. The selection of a sequence of candidate among a population to minimise a cost holds similarity to the Travelling Salesman Problem (TSP), well known and studied in optimisation literature. In the debris removal case, the J_2 dynamics conveys a time-variation in the debris orbital properties (orbital elements), transforming it into a Time-Dependent Travelling Salesman (TDTSP) problem. The combinatorial optimisation problem is formulated to select the optimal sequence of debris to minimise a multi-objective cost function. Generally, even in the case of single-objective minimisation, the present problem falls within the NP-class problem. Namely, the NP-class includes the optimisation problem with no known polynomial-time solving algorithm and are among the most difficult problems in operation research. As for the time-dependent travelling salesman problem, the multiple ADR selection is NP-hard and requires special care in the solution procedure. Methods for resolution of these combinatorial optimisation problem mainly fall into three main approaches:

- **Explicit enumeration**: This approach involves systematically assessing every combination in the combinatorial optimisation problem to guarantee the discovery of the best solution. However, as the problem's size grows, the number of possible combinations rapidly make the problem numerically intractable.
- **Implicit enumeration**: The exploration of the feasible space is performed with branch and cut or branch and bound methods to search for the optimal solution. An exponential growth of problem computational complexity for such algorithms is expected in function of the problem size.
- **Stochastic programming methods**: These approach involves heuristic methods such as genetic algorithm, simulated annealing, ant-colony optimisation. These algorithms rely on a limitation of the combination evaluated according to a specific heuristic to tackle large scale problem with a limited computational time compared to the explicit and implicit enumeration methods. Therefore, the global optimum is not guaranteed to be found, but rather approximate optima in a feasible computational time.

In this work a genetic algorithm is selected to approach the optimisation problem. This has been selected thanks to its feasibility in handling large scale problems with reasonable computational expense. The debris selection problem is defined considering a fixed number of debris N to be removed from a considered population, and is formulated in general as follows:

$$\min_{\boldsymbol{X}} [J_1(\boldsymbol{X}), J_2(\boldsymbol{X}))]^T \tag{17}$$

s.t.

$$g_m(\boldsymbol{X}) \leqslant 0 \quad \text{for} \quad m = 1, .., M$$
$$h_p(\boldsymbol{X}) = 0 \quad \text{for} \quad p = 1, \ldots, P$$

where $\boldsymbol{X}$ is vector variable to be optimised, $J_1(\boldsymbol{X})$ and $J_2(\boldsymbol{X})$ the two objective functions, and the $g_m(\boldsymbol{X})$ and $h_p(\boldsymbol{X})$ functions are the inequality and equality constraints. The optimisation problem of this study considers the optimisation variable $\boldsymbol{X} \in \mathbb{N}^N$ as variable of fixed size N of natural numbers that corresponds to the sequence of the debris object labels considered in the multiple ADR removal sequence. The objective functions are defined as follows:

$$\begin{cases} J_1(\boldsymbol{X}) = m_{p,tot} \\ J_2(\boldsymbol{X}) = -\sum_{i}^{N} I_{ADR,i} \end{cases} \tag{18}$$

which represent the total propellant mass $m_{p,tot}$ used during the sequence of removal and the negative of cumulative ADR index of the objects retrieved. The minus sign is introduced since the mission design tool shall prioritize targets with high cumulative ADR index, thus more interesting and feasible to be removed. As constraints, only inequality constraints are imposed, conveying a limit in the total time of flight for the overall mission:

$$g(\boldsymbol{X}) = TOF(\boldsymbol{X}) < T_{lim} \tag{19}$$

The time of flight function $TOF(\boldsymbol{X})$ is computed considering the natural drift due to J_2 required to transfer between two subsequent debris of the sequence. The mission time limit T_{lim} is set equal to 5 years in this work. The multi-objective optimisation problem described above is solved by computing the pareto front of solutions with respect to the cost functions of Eqs. 18. The solutions of this NP-hard combinatorial multi-objective optimisation problem are obtained considering a genetic algorithm heuristic. In particular a controlled elitist genetic algorithm, a variant of the NSGA-II algorithm Deb et al. (2002, 2006) is used, implemented in the MATLAB function *gamultiobj.m* Deb (2001). The algorithm creates the pareto front of non-dominated solutions for the ADR sequences in the two cost functions space.

6. Simulation results

In this section, we present the results generated by the multi-objective mission design tool for multiple ADR missions across different scenarios. Three distinct mission cases are defined, each representing a specific driver and the expected outcomes of implementing an ADR mission from the perspective of a mission designer. Specifically, the following mission cases are considered, each with a differently tuned ADR index:

- *Mission case* 1 - *Balanced ADR mission*: in this scenario the ADR index comprehends the contributions from all its sub-indices, namely the environmental, economical and operability. Here the mission designer seeks for a balanced solution which is capable of acting effectively as mitigation of the in-orbit collision risk in highly valuable orbital region, while accounting for the feasibility of capture of each target.
- *Mission case* 2 - *Debris collision risk mitigation*: in this scenario the ADR index comprehends the environmental and the economical contributions to convey a need of the mission designer to maximise the mitigation of collision risk in orbit for both the current population and the space environment in the long term.
- *Mission case* 3 - *Debris mitigation as technological demonstration*: in this scenario the ADR index comprehends the contributions of operation feasibility and of environmental effect. Here the mission designer seeks for a solution which can achieve a mitigation effect on the environment but with limited complications from the proximity operations point of view, i.e. early technological demonstrations of ADR.

For all test cases, a servicer with an initial wet mass of 2500 kg is assumed, equipped with an impulsive propulsion system with a specific impulse of 250 s. Additionally, the mission architecture assumes that the launcher can inject the servicer directly into the orbit of the first debris target, thus neglecting any transfer cost from an initial parking orbit. The ADR mission design tool simulates the removal of three debris targets. The population of objects considered is located in the region with a semi-major axis between 6800 km and 8000 km, and an inclination between 85 and 110 degrees. The vicinity of the SSO region was selected as a representative example, although objects in other inclination bands may be of interest. Substantial inclination changes are impractical within a single mission sequence due to their high propellant cost. Consequently, constraining the initial population's inclination range is advised to reduce the computational burden of the multi-objective optimization and to prevent the algorithm from exploring infeasible solutions that cause large inclination manoeuvres. For each test case, the multi-objective optimization genetic algorithm is run ten times to generate a comprehensive representation of the Pareto front of solutions. The parameters used for the genetic algorithm are reported in Table 3.

6.1. Mission case 1

The weights used in the ADR index definition of Eq. 1 for the first mission case are reported in Table 4. The test case represents a mission design where the removal of targets equally prioritise all the contribution of the ADR index.

The multi-objective optimisation problem is solved over 10 runs exploiting the genetic algorithm and the superimposition of the pareto front of solutions of the runs is shown in Fig. 13. Three different solution are highlighted with colored markers, which represent peculiar conditions of the ADR mission found. With a red marker, a solution in the low-end section of propellant expenditure is shown

Table 3
Parameters used in the ADR mission tool simulation for the multi-objective genetic algorithm.

Population size	5000
Maximum generations	10000
Maximum stall generations	50
Cost function tolerance	1e-6
Constraint function tolerance	1e-3
Cross-over fraction	65 %
Pareto fraction	40 %
Selection function	*tournament*
Distance measure function	*distance crowding*
Non linear constraint algorithm	*penalty*

Table 4
Weights selected for the ADR index associated to the test case 1 - balanced ADR mission.

w_{env} [–]	w_E [–]	w_{op} [–]
1	1	10

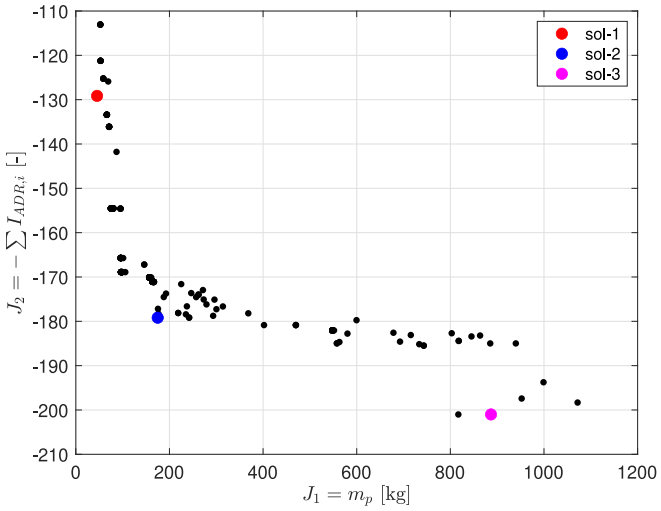

Fig. 13. Pareto front of optimisation solutions for test case 1 - balanced ADR mission.

and the debris sequence is reported in Table 5. It can be noted that the objects taken are all in the same orbital region, thus the transfer strategy used yields extremely low propellant values. However, this solution results in a cumulative ADR index which is low in absolute value. Furthermore, the object selected are of limited mass, thus limiting the propellant expenditure to perform de-orbiting. On the other hand, the solution highlighted in blue in Fig. 13 corresponds to larger cumulative index values, but still with moderate propellant cost. In this case, as reported in Table 6, the object selected are still of moderate mass, but are characterised by large operability and economical index. Therefore, it correspond to a solution where the removal targets are easy to be approached and captured and occupy orbital region of high commercial interest. Fig. 14 show the polar plot of the evolution of the RAAN and semi-major axis over time due to the J_2 natural drift and altitude changes manoeuvres involved in the first (top) and second (bottom) transfer of the solution highlighted in blue in Fig. 13 and with sequence of Table 6. Specifically, it can be noted how in the transfer strategy of RAAN drift for plane matching, after the designed drifting time, the RAAN of the two objects naturally match thanks to the differential perturbations induced by the Earth second zonal harmonic J2. Once the orbital plane is matched, the semi-major axis difference is also compensated with the Hohmann transfer to complete the orbit matching between the two consecutive target objects.

In general, for the balanced ADR mission case the pareto solutions which show low and moderate propellant consumption prioritise smaller objects with larger operational and economical index. Lastly, in the solution highlighted in magenta in Fig. 13 a large target, e.g. Envisat, is included in the sequence to reach higher cumulative ADR index, adding the contribution of high environmental contribution in the index. For this solution a propellant expenditure of around 742 kilograms is found. The full sequence, orbital location and associated sub-indeces for the objects of this last solution are reported in Table 7.

6.2. Mission case 2

The second mission case studied in this paper represent a mission where the environmental and economical contributions are prioritised. The weights selected in the index Eq. 1 are reported in Table 8.

Table 5
Sequence solution highlighted in red in the pareto front of test case 1 of Fig. 13. Propellant used for the transfer and deorbit strategy within this sequence is equal to 45.37 kg.

NORAD	Type	Name	M [kg]	a [km]	i [deg]	Ω [deg]	I_{env} [–]	I_{op} [–]	I_E [–]
55059	PL	Orbiter SN1	200	6819	97.417	296.3	0.00012	2.43	27.77
59677	PL	Haiwangxing-01	239	6857	97.399	306.8	0.00068	0.24	34.73
55090	PL	Chimera LEO-1	270	6833	97.420	296.1	0.00055	1.21	27.77

Table 6
Sequence solution highlighted in blue in the pareto front of test case 1 of Fig. 13. Propellant used for the transfer and deorbit strategy within this sequence is equal to 165.11 kg.

NORAD	Type	Name	M [kg]	a [km]	i [deg]	Ω [deg]	I_{env} [–]	I_{op} [–]	I_E [–]
3522	RB	Star 37B (T-Burner II)	154	7168	98.722	7.5	0.0401	2.83	30.36
6276	RB	Star 26B (T-Burner IIA)	115	7197	98.539	45.9	0.0228	3.05	30.00
28891	PL	Topsat	115	7061	98.220	358.4	0.0031	2.78	32.90

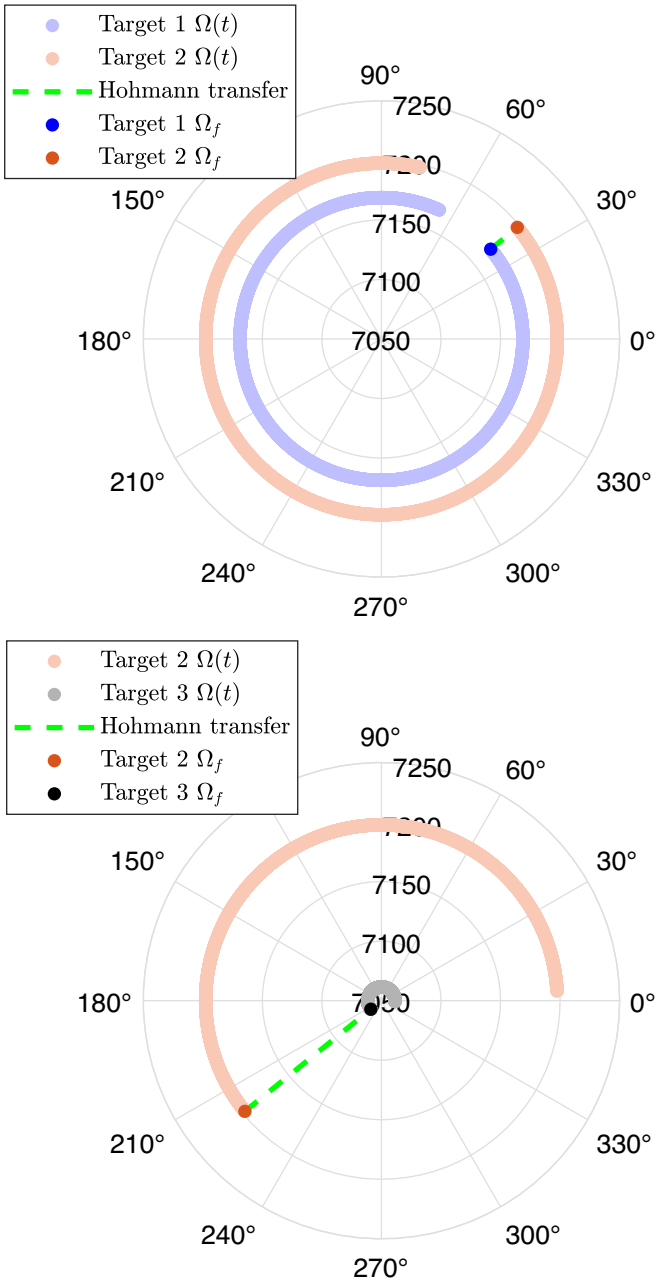

Fig. 14. Polar plot of first transfer (top) and second transfer (bottom) displaying the evolution of RAAN due to the natural J_2 induced drift and the altitude change performed with Hohmann transfer.

Again, the solution of the pareto front obtained for 10 runs of the multi-objective optimisation algorithm are super-imposed displayed in Fig. 15. The behaviour similar

Table 8
Weights selected for the ADR index associated to the test case 2 - Debris collision risk mitigation.

w_{env} [–]	w_E [–]	w_{op} [–]
1	1	0

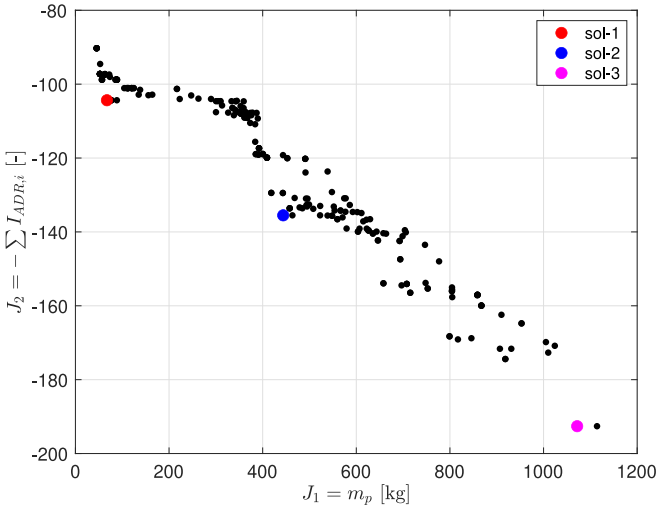

Fig. 15. Pareto front of optimisation solutions for test case 2 - Debris collision risk mitigation mission.

to the first mission case where the high ADR indexes sequences are related to higher propellant expenditure is still evident. The cause of this behaviour is twofold: (1) the population of debris used which does not have any orbital region with high density of large objects with high environmental index, and (2) in general objects with larger mass, thus with a larger environmental index, require a larger amount of propellant mass to be deorbited. Interesting to note is also that the pareto solution highlighted in red in Fig. 15, which refers to low propellant consumption but low cumulative ADR index, has debris objects selected similar to the same solutions highlighted in test case 1, as reported in Table 9. Particularly, relatively small mass debris within the same orbital region at low altitude SSO are inside this sequence.

Table 10 reports the debris objects in the sequence highlighted in blue in the pareto front of solutions in Fig. 15, selected a good compromise in the pareto front between cumulative ADR index and propellant used. Table 11

Table 7
Sequence solution highlighted in magenta in the pareto front of test case 1 of Fig. 13. Propellant used for the transfer and deorbit strategy within this sequence is equal to 742.48 kg.

NORAD	Type	Name	M [kg]	a [km]	i [deg]	Ω [deg]	I_{env} [–]	I_{op} [–]	I_E [–]
27386	PL	Envisat	8110	7141	98.2878	192.1	46.69	0.268	22.14
28050	RB	PSLV fourth stage (PS4)	920	7212	98.969	190.4	0.921	2.87	27.68
33313	PL	Trochia (RapidEye-5)	152	6949	97.483	269.4	0.001	2.51	31.58

Table 9
Sequence solution highlighted in red in the pareto front of mission case 2 of Fig. 15. Propellant used for the transfer and deorbit strategy within this sequence is equal to 76.54 kg.

NORAD	Type	Name	M [kg]	a [km]	i [deg]	Ω [deg]	I_{env} [–]	I_{op} [–]	I_E [–]
58825	PL	Taijing 2–02	100	6886	97.506	306.9	2.9e-05	0.125	34.74
59677	PL	Haiwangxing-01	239	6857	97.400	306.8	0.0007	0.244	34.74
48843	PL	Beijing-3	3000	6874	97.400	310.4	0.149	0.176	34.74

Table 10
Sequence solution highlighted in blue in the pareto front of mission case 2 of Fig. 15. Propellant used for the transfer and deorbit strategy within this sequence is equal to 463.51 kg.

NORAD	Type	Name	M [kg]	a [km]	i [deg]	Ω [deg]	I_{env} [–]	I_{op} [–]	I_E [–]
27386	PL	Envisat	8110	7141	98.288	192.1	46.69	0.268	22.14
31117	PL	Egyptsat 1 (MisrSat 1)	100	7018	97.968	180.5	0.0023	0.262	33.26
26619	PL	EO-1	588	7049	98.022	187.2	0.144	1.256	33.26

Table 11
Sequence solution highlighted in magenta in the pareto front of mission case 2 of Fig. 15. Propellant used for the transfer and deorbit strategy within this sequence is equal to 1071.79 kg.

NORAD	Type	Name	M [kg]	a [km]	i [deg]	Ω [deg]	I_{env} [–]	I_{op} [–]	I_E [–]
25400	RB	Zenit-2 s stage	8226	7183	98.746	173.7	39.04	0.0252	30.36
33272	PL	Cosmos-2441	7000	7095	98.244	176.0	21.47	0.0067	32.90
27386	PL	Envisat	8110	7141	98.288	192.1	46.69	0.268	22.14

shows instead the debris objects in the sequence highlighted in magenta in the pareto front of solutions in Fig. 15, representing the best solution in terms of cumulative ADR index in the pareto front. The mission include large debris objects in SSO which, if remove, will greatly mitigate the risk of the current and long term space environment.

6.3. Mission case 3

In this final test case, we examine a scenario that simulates an early future mission within the ADR domain. Therefore, there is emphasis on assessing technological and operational feasibilities, as these initial missions serve as crucial demonstrations of their capabilities in orbit for the first time. The associated weights for the ADR index in this test case are outlined in Table 12.

Fig. 16 shows the solutions of the pareto fronts for the 10 runs of the multi-objective optimisation algorithm for mission case 3. Again, three solutions have been highlighted and sequence reported in Tables 13–15. Also in this case, the behaviour of choosing objects with large environmental index in solutions where there is a greater cumulative ADR index and, thus, greater propellant expenditure is observed. Of course it is possible for the mission planner, thanks to the flexibility of the tool, to tailor the outcome of the mission to its specific needs. For example, if the maturity of the demo mission is lower, and cannot afford to capture large objects as in this test case, the relative

Table 12
Weights selected for the ADR index associated to the mission case 3 - debris mitigation as technological demonstration mission.

w_{env} [–]	w_E [–]	w_{op} [–]
1	0	10

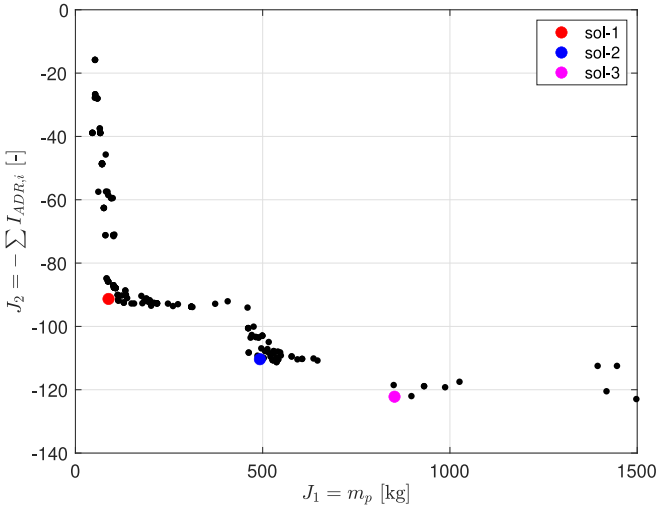

Fig. 16. Pareto front of optimisation solutions for test case 3 - debris mitigation as technological demonstration mission.

Table 13
Sequence solution highlighted in red in the pareto front of mission case 3 of Fig. 16. Propellant used for the transfer and deorbit strategy within this sequence is equal to 88.41 kg.

NORAD	Type	Name	M [kg]	a [km]	i [deg]	Ω [deg]	I_{env} [–]	I_{op} [–]	I_E [–]
5556	RB	Star 26B (T-Burner IIA)	115	7191	99.013	169.9	0.0221	3.10	0
28050	RB	PSLV fourth stage (PS4)	920	7212	98.969	190.4	0.9213	2.87	27.67
7219	RB	Star 26B (T-Burner IIA)	115	7184	98.980	165.8	0.0221	3.07	0

Table 14
Sequence solution highlighted in blue in the pareto front of mission case 3 of Fig. 16. Propellant used for the transfer and deorbit strategy within this sequence is equal to 492.64 kg.

NORAD	Type	Name	M [kg]	a [km]	i [deg]	Ω [deg]	I_{env} [–]	I_{op} [–]	I_E [–]
27386	PL	Envisat	8110	7141	98.288	192.1	46.6903	0.27	22.14
4513	RB	Star 37B (T-Burner II)	154	7156	98.877	171.8	0.04007	3.11	0
28637	RB	ORION 38	410	7230	98.743	233.4	0.2296	2.96	28.69

Table 15
Sequence solution highlighted in magenta in the pareto front of mission case 3 of Fig. 16. Propellant used for the transfer and deorbit strategy within this sequence is equal to 818.88 kg.

NORAD	Type	Name	M [kg]	a [km]	i [deg]	Ω [deg]	I_{env} [–]	I_{op} [–]	I_E [–]
4513	RB	Star 37B (T-Burner II)	154	7156	98.877	171.8	0.04007	3.11	0
25400	RB	Zenit-2 s stage	8226	7184	98.747	173.7	39.0377	0.025	30.36
27386	PL	Envisat	8110	7141	98.288	192.1	46.69	0.268	22.14

weight between operability and environmental index should be changed.

7. Conclusions

This paper has presented an innovative ranking framework for active debris removal missions target's selection, and a flexible mission design tool to plan these mission efficiently. The ranking definition incorporates an evaluation not only of the object's danger to the debris environment in terms of collision risk but also considerations regarding the technical feasibility of its capture and the commercial interest for current satellite operators to remove it from its current orbital region. Moreover, the mission design tool presented is capable to address in a flexible manner the need of different mission scenarios that the mission planner may require. The tool implements the generation of pareto front through multi-objective optimisation of the debris sequence with a genetic algorithm considering propellant cost of the mission and the cumulative index of the removed objects. Application of this framework to three different mission cases is presented, where missions with different priorities have been considered. As future work stemming from this paper, two domains can be identified. Firstly, in the ranking framework definition, more advanced index formulations to more accurately model the operational and environmental impact of debris are envisioned. In particular, future work will investigate methods to overcome the lack of data-and its limited representativeness-regarding the rotational states of many in-orbit objects, as well as studies on the formulation of operability indices for different capture methods discussed in the literature. An interesting impact will also arise in the considerations of the effects of just-in-time collision avoidance and ground-based non-contact removal of small debris in the evaluation of the true environmental risk of the considered target debris. Concerning the mission design tool, in this paper the development focused on capturing the behaviour in a multi-objective optimisation by simultaneously considering the ADR index and mission cost as metrics. Therefore, a choice on the mission architecture and transfer methods was made in this regard. Future investigation to find better solutions in terms of absolute cost of the mission should focus on the development of different architectures and different transfers methods within the sequence, i.e. low thrust transfers and drift orbits methods for RAAN compensation.

Declaration of competing interest

The authors declare that they have no known competing financial interests or personal relationships that could have appeared to influence the work reported in this paper.

Acknowledgements

The research leading to these results has received funding from the European Research Council (ERC) under the European Union's Horizon2020 research and innovation programme as part of project COMPASS (Grant agreement No 679086).

References

ESA DISCOS Database. https://discosweb.esoc.esa.int. Accessed: 2023-10-01.

MMT Telescope Light Curves. http://mmt9.ru/satellites/. Accessed: 2020-12-01.

SpaceTrack website. https://www.space-track.org/. Accessed: 2023-10-01.

Adilov, N., Braun, V., Alexander, P. et al., 2023. An estimate of expected economic losses from satellite collisions with orbital debris. J. Space Saf. Eng., 10(1), 66–69. https://www.sciencedirect.com/science/article/pii/S2468896723000022. doi: 10.1016/j.jsse.2023.01.002.

Allworth, J., Windrim, L., Wardman, J. et al., 2020a. Development of a high fidelity simulator for generalised photometric based space object classification using machine learning. arXiv preprint arXiv:2004.12270.

Allworth, J., Windrim, L., Wardman, J. et al., 2020b. Development of a high fidelity simulator for generalised photometric based space object classification using machine learning. arXiv preprint arXiv:2004.12270.

Anselmo, L., Pardini, C., 2015. Compliance of the italian satellites in low earth orbit with the end-of-life disposal guidelines for space debris mitigation and ranking of their long-term criticality for the environment. Acta Astronaut. 114, 93–100. https://doi.org/10.1016/j.actaastro.2015.04.024.

Anselmo, L., Pardini, C., 2016. Ranking upper stages in low earth orbit for active removal. Acta Astronaut. 122, 19–27. https://doi.org/10.1016/j.actaastro.2016.01.019.

Anselmo, L., Pardini, C., 2017. An index for ranking active debris removal targets in leo. In: Proc. 7th European Conference on Space Debris. Darmstadt, Germany.

Atarashi, E., Inoue, H., Fujii, G., 2024. Ultra-Close RPO on-orbit demonstration of ADRAS-J Program. In: Proceedings of the 75th International Astronautical Congress, IAC.

Barea, A., Urrutxua, H., Cadarso, L., 2020. Large-scale object selection and trajectory planning for multi-target space debris removal missions. Acta Astronaut., 170, 289–301.https://www.sciencedirect.com/science/article/pii/S0094576520300436. doi: 10.1016/j.actaastro.2020.01.032.

Biesbroek, R., Aziz, S., Wolahan, A., et al., 2021. The clearspace-1 mission: Esa and clearspace team up to remove debris. In: Proc. 8th European Conference on Space Debris.

Biesbroek, R., Innocenti, L., Wolahan, A., et al., 2017. e.Deorbit - ESA's active debris removal mission. In: Proc. 7th European Conference on Space Debris.

Blacketer, L.D.J., Lewis, H.G., Urrutxua, H., 2019. A technique for rotation vector position determination for tumbling rocket bodies. In: First International Orbital Debris Conference.

Bombardelli, C., Pelaez, J., 2011. Ion beam shepherd for contactless space debris removal. J. Guid., Control, Dynam., 34(3), 916–920. doi: 10.2514/1.51832. arXiv:https://doi.org/10.2514/1.51832.

Borelli, G., Gaias, G., Colombo, C., 2024. Guidance and control for safe contactless plume impingement operations to detumble an uncooperative spacecraft. Aerospace, 11(3).https://www.mdpi.com/2226-4310/11/3/224.

Braun, V., Horstmann, A., Lemmens, S., et al., 2021. Recent developments in space debris environment modelling, verification and validation with master. In: 8th European Conference on Space Debris, p. 18.

Braun, V., Schulz, E., Wiedemann, C., 2014. Cost estimation for the active debris removal of multiple priority targets.

Béal, S., Deschamps, M., Moulin, H., 2020. Taxing congestion of the space commons. Acta Astronaut., 177, 313–319.https://www.sciencedirect.com/science/article/pii/S009457652030463X. doi: 10.1016/j.actaastro.2020.07.036.

Bérend, N., Olive, X., 2016. Bi-objective optimization of a multiple-target active debris removal mission. Acta Astronaut., 122, 324–335.https://www.sciencedirect.com/science/article/pii/S0094576516000527. doi: 10.1016/j.actaastro.2016.02.005.

Casalino, L. ( ). Active debris removal missions with multiple targets. In: AIAA/AAS Astrodynamics Specialist Conference.https://arc.aiaa.org/doi/abs/10.2514/6.2014-4226. doi:10.2514/6.2014-4226. arXiv: https://arc.aiaa.org/doi/pdf/10.2514/6.2014-4226.

Cerf, M., 2013. Multiple space debris collecting mission—debris selection and trajectory optimization. J. Optim. Theory Appl. 156 (3), 761–796. https://doi.org/10.1007/s10957-012-0130-6.

Colombo, C., 2016. Planetary orbital dynamics (PlanODyn) suite for long term propagation in perturbed envirnoment. In: Proceedings of the 6th International Conference on Astrodynamics Tools and Techniques (ICATT) (2016).http://weekly.cnbnews.com/news/article.html?no=124000.

Colombo, C., Huang, S., Borelli, G., et al., 2021. Mission analysis and design for an active debris removal service for large constellations. In: 8th European Conference on Space Debris.

Colombo, C., Letizia, F., Trisolini, M., et al., 2017. Life cycle assessment indicator for space debris. In: 7th European Conference on Space Debris.

Colombo, C., Muciaccia, A., Giudici, L., et al., 2023. Tracking the health of the space debris environment with themis.

Colvin, J.T., Karcz, J., Wusk, G., 2023. Cost and benefit analysis of orbital debris remediation. In: Technical Report National Aeronautics and Space Administration (NASA) Washington, DC.

Deb, K., 2001. Multi-Objective Optimization using Evolutionary Algorithms. John Wiley & Sons Ltd, Chichester, England.

Deb, K., Agrawal, S., Pratap, A., et al., 2002. A fast and elitist multiobjective genetic algorithm: Nsga-ii. IEEE Trans. Evol. Comput. 6, 182–197, URL: https://api.semanticscholar.org/CorpusID:9914171.

Di Carlo, M., Romero Martin, J.M., Vasile, M., 2017. Automatic trajectory planning for low-thrust active removal mission in low-earth orbit. Adv. Space Res., 59(5), 1234–1258.https://www.sciencedirect.com/science/article/pii/S0273117716306767. doi: 10.1016/j.asr.2016.11.033.

ESA Space Debris Office, 2024. ESA'S ANNUAL SPACE ENVIRONMENT REPORT. Technical Report European Space Agency.

Federici, L., Zavoli, A., Colasurdo, G., 2019a. A time-dependent tsp formulation for the design of an active debris removal mission using simulated annealing. arXiv preprint arXiv:1909.10427.

Federici, L., Zavoli, A., Colasurdo, G., 2021. On the use of a* search for active debris removal mission planning. J. Space Saf. Eng., 8(3), 245–255.https://www.sciencedirect.com/science/article/pii/S2468896721000628. doi: 10.1016/j.jsse.2021.07.003.

Federici, L., Zavoli, A., Colasurdo, G. et al., 2019b. Impulsive multi-rendezvous trajectory design an optimization. In: 8th European Conference for Aeronautics and Space Sciences (EUCASS), Madrid, Spain, pp. 1–4.

Floher, T., Lemmens, S., Bastida Virgili, B. et al., 2013. Discos – current status and future developments. In: Proceedings of the 6h European Conference on Space Debris, ESOC, Darmstadt, Germany, 2013 (August), 1–7.

Forshaw, J.L., Aglietti, G.S., Navarathinam, N. et al., 2016. Removedebris: An in-orbit active debris removal demonstration mission. Acta Astronaut., 127, 448–463.https://www.sciencedirect.com/science/article/pii/S009457651530117X. doi: 10.1016/j.actaastro.2016.06.018.

Furfaro, R., Linares, R., Reddy, V., 2018. Space objects classification via light-curve measurements: deep convolutional neural networks and model-based transfer learning. In: AMOS Technologies Conference, Maui Economic Development Board.

Giudici, L., Colombo, C., Letizia, F., 2024. Optimal active debris removal sequence identification through combined debris index analysis and long-term projection of the orbital environment. In: Proceedings of the 75th International Astronautical Congress.

Hallmann, M., Schlotterer, M., Heidecker, A. et al., 2017. Gtoc 9, multiple space debris rendezvous trajectory design in the j2 environment.
Huang, S., Colombo, C., Gonzalo, J.L., et al., 2020. Preliminary mission analysis of active debris removal service for large constellations. In: Proceedings of the 71st International Astronautical Congress (IAC).
Izzo, D., Maertens, M., 2018. The Kessler Run: On the Design of the GTOC9 Challenge. Acta Futura 11, 11–24.
Jaekel, S., Lampariello, R., Rackl, W., et al., 2018. Design and operational elements of the robotic subsystem for the e.deorbit debris removal mission. Front. Robot. AI 5. https://doi.org/10.3389/frobt.2018.00100, URL: https://www.frontiersin.org/articles/10.3389/frobt.2018.00100.
Johnson, N.L., Krisko, P.H., Liou, J.C., et al., 2001. NASA's new breakup model of EVOLVE 4.0. Adv. Space Res. 28 (9), 1377–1384. https://doi.org/10.1016/S0273-1177(01)00423-9.
Konak, A., Coit, D.W., Smith, A.E., 2006. Multi-objective optimization using genetic algorithms: a tutorial. Reliab. Eng. Syst. Saf., 91(9), 992–1007.https://www.sciencedirect.com/science/article/pii/S0951832005002012. doi: 10.1016/j.ress.2005.11.018. Special Issue - Genetic Algorithms and Reliability.
Kucharski, D., Kirchner, G., Koidl, F., et al., 2014. Attitude and spin period of space debris envisat measured by satellite laser ranging. IEEE Trans. Geosci. Remote Sens. 52 (12), 7651–7657.
Kunstadter, C., 2021. Collision risk: The insurer's view, from measurements to understanding. In: MASTER Modelling Workshop (virtual) presentation. European Space Agency.
Lemmens, S., Krag, H., Rosebrock, J., et al., 2013. Radar mappings for attitude analysis of objects in orbit. In: Proc. 6th European Conference on Space Debris, pp. 20–24.
Letizia, F., Colombo, C., Lewis, H.G., et al., 2016. Assessment of breakup severity on operational satellites. Adv. Space Res. 58 (7), 1255–1274. https://doi.org/10.1016/j.asr.2016.05.036.
Letizia, F., Colombo, C., Lewis, H.G., et al., 2017. Extending the ECOB space debris index with fragmentation risk estimation. 7th European Conference on Space Debris, Darmstadt, Germany, 417, pp. 1–10.
Liou, J.C., 2011. An active debris removal parametric study for LEO environment remediation. Adv. Space Res. 47 (11), 1865–1876. https://doi.org/10.1016/j.asr.2011.02.003.
Liou, J.C., Johnson, N.L., 2009. A sensitivity study of the effectiveness of active debris removal in LEO. Acta Astronaut. 64 (2–3), 236–243. https://doi.org/10.1016/j.actaastro.2008.07.009.
Liu, Y., Yang, J. ( ). A multi-objective planning method for multi-debris active removal mission in leo. In: AIAA Guidance, Navigation, and Control Conference.https://arc.aiaa.org/doi/abs/10.2514/6.2017-1733. arXiv:https://arc.aiaa.org/doi/pdf/10.2514/6.2017-1733.
Macauley, M.K., 2015. The economics of space debris: Estimating the costs and benefits of debris mitigation. Acta Astronaut., 115, 160–164. https://www.sciencedirect.com/science/article/pii/S0094576515001873. doi: 10.1016/j.actaastro.2015.05.006.
Madakat, D., Morio, J., Vanderpooten, D., 2013. Biobjective planning of an active debris removal mission. Acta Astronaut., 84, 182–188. https://www.sciencedirect.com/science/article/pii/S0094576512004274. doi: 10.1016/j.actaastro.2012.10.038.
McKnight, D., Witner, R., Letizia, F., et al., 2021. Identifying the 50 statistically-most-concerning derelict objects in LEO. Acta Astronaut. 181 (January), 282–291. https://doi.org/10.1016/j.actaastro.2021.01.021.
Murakami, J., Hokamoto, S., 2010. Approach for optimal multi-rendezvous trajectory design for active debris removal. In: 61st International Astronautical Congress 2010, pp. 6013–6018, IAC 2010.
Nishida, S.-I., Kawamoto, S., 2011. Strategy for capturing of a tumbling space debris. Acta Astronaut., 68(1), 113–120.https://www.sciencedirect.com/science/article/pii/S0094576510002365. doi: 10.1016/j.actaastro.2010.06.045.
Oikonomidou, X., Braun, V., Lemmens, S., 2021. Guidelines for space debris and meteroid impact risk assessment with drama/midas. In: Proc. 8th European Conference on Space Debris.
Peters, T.V., Olmos, D.E., 2016. Cobra contactless detumbling. CEAS Space J. 8 (3), 143–165.
Petropoulos, A., Grebow, D., Jones, D., et al., 2018. Gtoc9: Results from the Jet Propulsion Laboratory (team JPL). Acta Futura 11, 25–35.
Rao, A., Burgess, M.G., Kaffine, D., 2020. Orbital-use fees could more than quadruple the value of the space industry. Proc. Nat. Acad. Sci. 117 (23), 12756–12762. https://doi.org/10.1073/pnas.1921260117, URL: https://www.pnas.org/doi/abs/10.1073/pnas.1921260117. arXiv:https://www.pnas.org/doi/pdf/10.1073/pnas.1921260117.
Rossi, A., Valsecchi, G., Alessi, E., 2015a. The criticality of spacecraft index. Adv. Space Res. 56 (3), 449–460.
Rossi, A., Valsecchi, G.B., Alessi, E.M., 2015b. The criticality of spacecraft index. Adv. Space Res. 56 (3), 449–460. https://doi.org/10.1016/j.asr.2015.02.027.
Sagnières, L.B., Sharf, I., 2019. Long-term rotational motion analysis and comparison to observations of the inoperative envisat. J. Guid., Control, Dynam. 42 (2), 364–376.
Schaub, H., Sternovsky, Z., 2013. Active space debris charging for contactless electrostatic disposal maneuvers. In: 6th European Conference on Space Debris.
Schildknecht, T., Linder, E., Silha, J., et al., 2015. Photometric monitoring of non-resolved space debris and databases of optical light curves. In: Advanced Maui Optical and Space Surveillance Technologies Conference, p. 25.
Shen, H.-X., Zhang, T.-J., Casalino, L. et al., 2018. Optimization of active debris removal missions with multiple targets. J. Spacecr. Rock., 55(1), 181–189. doi: 10.2514/1.A33883. arXiv:https://doi.org/10.2514/1.A33883.
Šilha, J., Pittet, J.-N., Hamara, M., et al., 2018. Apparent rotation properties of space debris extracted from photometric measurements. Adv. Space Res. 61 (3), 844–861.
Silha, J., Schildknecht, T., Pittet, J., et al., 2017. Debris attitude motion measurements and modelling by combining different observation techniques. In: Proc. 7th European Conference on Space Debris June. Darmstadt, Germany.
Šilha, J., Schildknecht, T., Pittet, J., et al., 2017. Extensive light curve database of astronomical institute of the university of bern. In: Proc. of 7th European Conference on Space Debris, Darmstadt, Germany.
Tsuno, K., Wada, S., Ogawa, T., et al., 2022. Laser ablation induced impulse study for removal of space debris mission using small satellite. Appl. Phys. A 128 (10), 932. https://doi.org/10.1007/s00339-022-05983-2.
Vananti, A., Guthruf, D., Lu, Y., et al., 2021. Estimation of reflective properties from light curves of a h2a rocket body. In: 8th European Conference on Space Debris, p. 51.
Viavattene, G., Devereux, E., Snelling, D. et al., 2022. Design of multiple space debris removal missions using machine learning. Acta Astronaut., 193, 277–286.https://www.sciencedirect.com/science/article/pii/S0094576521006974. doi: 10.1016/j.actaastro.2021.12.051.
Virgili, B.B., Krag, H., 2013a. Active debris removal for LEO missions. In: Proc. 6th European Conference on Space Debris April.
Virgili, B.B., Krag, H., 2013b. Criteria for the selection of targets for active debris removal. In: Proc. of 4th CEAS Air and Space Conference. https://doi.org/10.13140/2.1.4377.9845.
Xu, Y., Liu, X., He, R. et al., 2023. Active debris removal mission planning method based on machine learning. Mathematics, 11(6). https://www.mdpi.com/2227-7390/11/6/1419.
Yang, J., Hu, Y.H., Liu, Y. et al., 2018. A maximal-reward preliminary planning for multi-debris active removal mission in leo with a greedy heuristic method. Acta Astronaut., 149, 123–142.https://www.sciencedirect.com/science/article/pii/S0094576518303229. doi: 10.1016/j.actaastro.2018.05.040.
Yasaka, T., 2011. Can we have an end to the debris issue? In: 62nd International Astronautical Congress 2011, IAC 2011 (pp. 2197–2203). volume 3.
Zuiani, F., Vasile, M., 2012. Preliminary design of debris removal missions by means of simplified models for low-thrust, many-revolution transfers. Int. J. Aerospace Eng., 2012, 836250. doi:10.1155/2012/836250.